Protracted subduction of the European hyperextended margin revealed by rutile U-Pb geochronology across the Dora-Maira massif (W. Alps)

Tectonics

Guillaume Bonnet[1,2], Christian Chopin[3], Michele Locatelli[4], Andrew Kylander-Clark[1], Bradley R. Hacker[1]

[1] Department of Earth Science, University of California, Santa Barbara, Santa Barbara, CA, USA

[2] Sorbonne Université, CNRS-INSU, Institut des Sciences de la Terre Paris, ISTeP UMR 7193, F-75005 Paris, France

[3] Laboratoire de Géologie, École normale supérieure, CNRS, UMR8538, Université PSL, 75005 Paris, France

[4] Dipartimento di Scienze della Terra Ambiente e Vita, Università di Genova, Italy

Key points:

- Rutile U-Pb geochronology contrains peak metamorphism of Dora-Maira units younging downward in the nappe stack from ~40 to ~33 Ma
- Continuous and fast exhumation of subducted continental crust
- ~200 km hyperextended European margin prior to subduction

Abstract

The Dora-Maira massif is an archetypal nappe stack of subducted and exhumed upper crust. Slices of continental crust experienced metamorphism at upper blueschist to ultrahigh-pressure (UHP) eclogite-facies conditions. While the timing of peak metamorphism in the UHP unit has been extensively studied, little is known about the other units. In order to constrain the timing and conditions of high-pressure metamorphism, U-Pb-trace element analyses of rutile and titanite were carried out across the nappe stack. The data reveal Alpine peak metamorphic ages younging downwards in the stack, from ~40 Ma to ~33 Ma. Greenschist-facies retrogression of the whole massif occurred at ~32-31 Ma, after high-pressure metamorphism of the lowermost unit (Sanfront-Pinerolo Unit). Tectonic implications include (1) continuous and fast exhumation of subducted continental crust, (2) long-lived subduction from ~60 Ma until ~33 Ma of the distal European margin, reconstructed to be a hyperextended margin spread over ~130 km for the Dora-Maira massif alone, and (3) the initiation of continental collision synchronous with the end of high-pressure metamorphism.

1. Introduction

The occurrence of continental rocks metamorphosed at high-pressure, low-temperature conditions has been interpreted as resulting from continental subduction, which occurs when continental margins are carried to depth after the subduction of dense oceanic lithosphere (Chopin, 1984; Liou et al., 2004). Exhumed subducted continental terranes occur as two endmembers, involving distinct mechanisms of subduction and exhumation (Kylander-Clark et al., 2012): (1) large, mostly coherent continental units (former downgoing plates; e.g, Western Gneiss Region, Norway, Wain, 1997; Sulu-Dabie belt, China, Hacker et al., 2004), or (2) small units organized in nappe stacks (e.g., Oman, Alpine Corsica; Agard and Vitale-Brovarone, 2013). Relics of ultra-high-pressure metamorphism (in the coesite or diamond stability fields) have been identified in some of these examples (e.g., Chopin, 2003; Hacker and Gerya, 2013). Once sliced off the downgoing plate (cf. Agard et al., 2009, 2018), the buoyant continental rocks are expected to be exhumed continuously and fast.
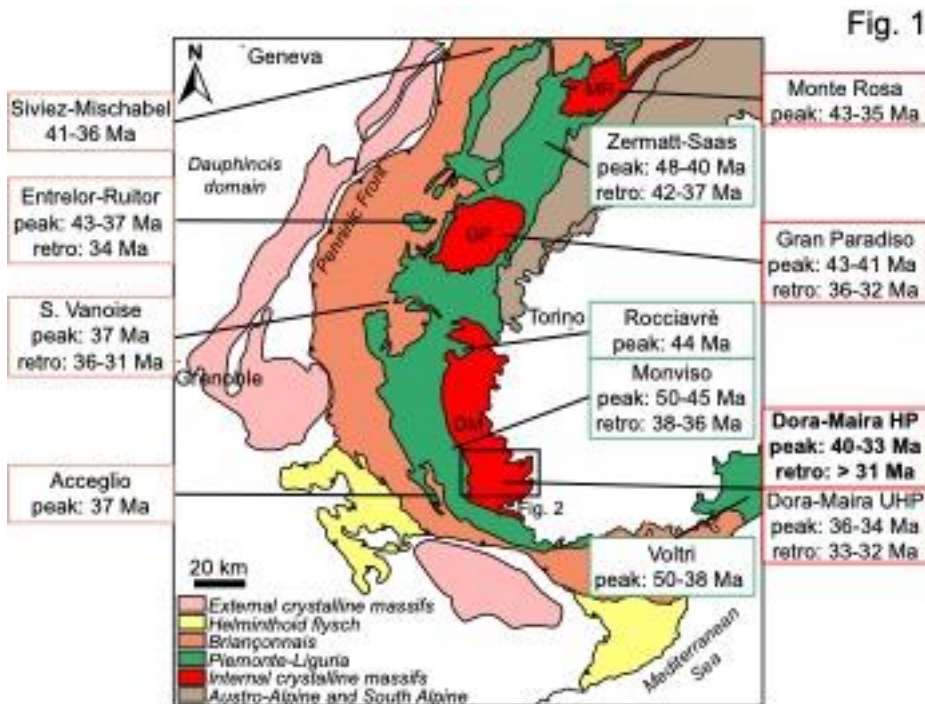

Fig. 1: Simplified geological map of the western Alps, showing ages of Alpine high-pressure metamorphism of distinct structural domains and massifs, from the internal Briançonnais and Internal Crystalline Massifs and the Piemonte-Liguria domains. MR = Monte Rosa, GP = Gran Paradiso, DM = Dora-Maira. The rectangle in southern Dora-Maira shows the location of the map on Fig. 2. "peak" indicates the commonly admitted range of ages for peak metamorphism, "retro" indicates the range of ages of retrograde metamorphism. See references in text and in Supporting Table S1. Bold values for Dora-Maira are from this study.

The Western Alps (Fig. 1) constitute an ideal area for studying continental subduction: the Briançonnais terrane, interpreted as the passive margin of the European plate (e.g., Ballèvre et al., 2020), was metamorphosed at high-pressure, low-temperature conditions, while it was subducted below the Adria plate (e.g., Debelmas and Lemoine, 1970; Dal Piaz and Lombardo, 1986; Ganne et al., 2007, Lanari et al., 2012). Briançonnais units are exposed between the Penninic Front (i.e., the main collision-related thrust fault in the Western Alps, Ceriani et al., 2001) and the Piemonte-Liguria ocean-derived domain, in the Briançonnais domain *sensu stricto*. Three continental massifs are exposed farther east as tectonic windows below the Piemonte-Liguria domain and are interpreted by most authors as belonging to the same paleogeographic domain as the Briançonnais, i.e., European basement subducted below Adria. These three massifs, referred to as the Internal Crystalline Massifs, are from north to south: the Monte Rosa, Gran Paradiso and Dora-Maira massifs. The Dora-Maira massif (Vialon, 1966) is the largest and most studied, mainly owing to the first discovery there of coesite in a subduction-related terrane (Chopin et al., 1984). However, the coesite-bearing whiteschists focused most of the scientific attention, despite representing very small volumes in the coesite-bearing unit, which itself accounts for only ~ 3% of all Dora-Maira exposures. The bulk (~ 97%) of the Dora-Maira massif is constituted by tectonic slivers (mainly of continental affinity) recording different pressure-temperature (P-T) conditions (Pognante and Sandrone, 1989; Chopin et al., 1991; Henry et al., 1993; Groppo et al., 2019) and likely reflecting distinct subduction histories. Therefore, continental subduction is likely to have lasted longer than the short period of coesite-grade metamorphism (Rubatto and Hermann, 2001). In this study, the timing of peak metamorphism in each unit of the Dora-Maira nappe stack is assessed by U-Pb geochronology on rutile (an abundant mineral of various high-pressure assemblages across all units), to better understand the subduction and exhumation dynamics of slices of continental crust. This helps constrain the duration of continental subduction, a transient stage between oceanic subduction and continental collision.

2. Geological context

2.1. Structure and metamorphic conditions of the massif

The Dora-Maira massif occupies an internal position in the Alpine orogenic wedge (Fig. 1). It consists of large exposures of continent-derived units (orthogneisses, with their host Paleozoic metamorphic country rocks, and minor Mesozoic sedimentary cover) between the Dora Riparia River (north) and the Maira River (south). Most studies focus on a west-east transect following the crest between the Po and Varaita valleys in the southern part of the Dora-Maira massif where coesite was found (Chopin, 1984). On this transect, the Dora-Maira massif was described as a nappe-stack with three main bodies (Michard, 1967; Henry et al., 1993) (from bottom to top; Fig. 2): (1) the Sanfront-Pinerolo Unit (SPU, with graphitic schists of likely Carboniferous age and minor Triassic carbonates),

(2) the main Dora-Maira basement complex (consisting almost exclusively of orthogneisses with their country rocks), and (3) the Dronero-Sampeyre unit (DSU, with Permo-Carboniferous graphitic schist and Permo-Triassic quartzite and conglomerate). The base of the Sanfront-Pinerolo unit is not exposed, making it the structurally lowermost unit in the internal Alps. Within the main Dora-Maira basement complex, several subunits have been identified, locally separated by sheared (mainly Triassic) metasedimentary slivers (Henry et al., 1993; Compagnoni and Rolfo, 2003; Compagnoni et al., 2012). They are, from bottom to top: the San Chiaffredo Unit (SCU), the Brossasco-Isasca Unit (BIU), the Rocca Solei Unit (RSU), and the Ricordone Unit (RU), the latter three corresponding to Units 1, 2 and 3 of Henry et al. (1993). At the base of the Dronero-Sampeyre unit, the Ophiolitiferous Band (OB), or Valmala shear zone (Henry et al., 1993; Balestro et al., 2020) consists of mixed continental and oceanic rocks (including orthogneisses, calcschists, metabasalts and serpentinites). Above the Dronero-Sampeyre unit, one or several slivers of mixed oceanic (Jurassic to Cretaceous calcschists) and continental (Triassic to upper Cretaceous) metasediments are intercalated below the Monviso metaophiolite complex (Balestro et al., 2011, 2015). These units have been mapped and named here as the Cima di Crosa unit (CCU, Fig. 2).

The Brossasco-Isasca unit is the only unit where UHP metamorphism has been recognized, and peak P-T conditions of ~3.5-4.0 GPa and 700-750°C (Fig.3) have been estimated from a variety of lithologies in the unit, including coesite-pyrope-bearing whiteschist (e.g., Chopin, 1984; Schertl et al., 1991; Sharp et al., 1993; Hermann, 2003; Ferrando et al., 2009; Campomenosi et al., 2021), mafic eclogite (Chopin et al., 1991; Kienast et al., 1991; Chopin and Schertl, 1999; Nowlan et al., 2000; Groppo et al., 2007), metapelite (Chopin et al., 1991; Groppo et al., 2019), and impure marble (Castelli et al., 2007; Ferrando et al., 2017). Relics of UHP metamorphism have also been found in country-rock orthogneiss, including grossular-rich garnet in equilibrium with rutile (Chopin et al., 1991), coronitic UHP assemblages including Ca-Eskola pyroxene (Bruno et al., 2001, 2002), and inclusions of coesite within metamorphic zircon rim (Xiong et al., 2021). The scarcity of such relics is due to the limited reactivity of granitic protoliths, that were not much deformed at great depth (Biino and Compagnoni, 1992; Lenze and Stöckhert, 2007), and to the strong overprint due to deformation during retrogression under greenschist-facies conditions.
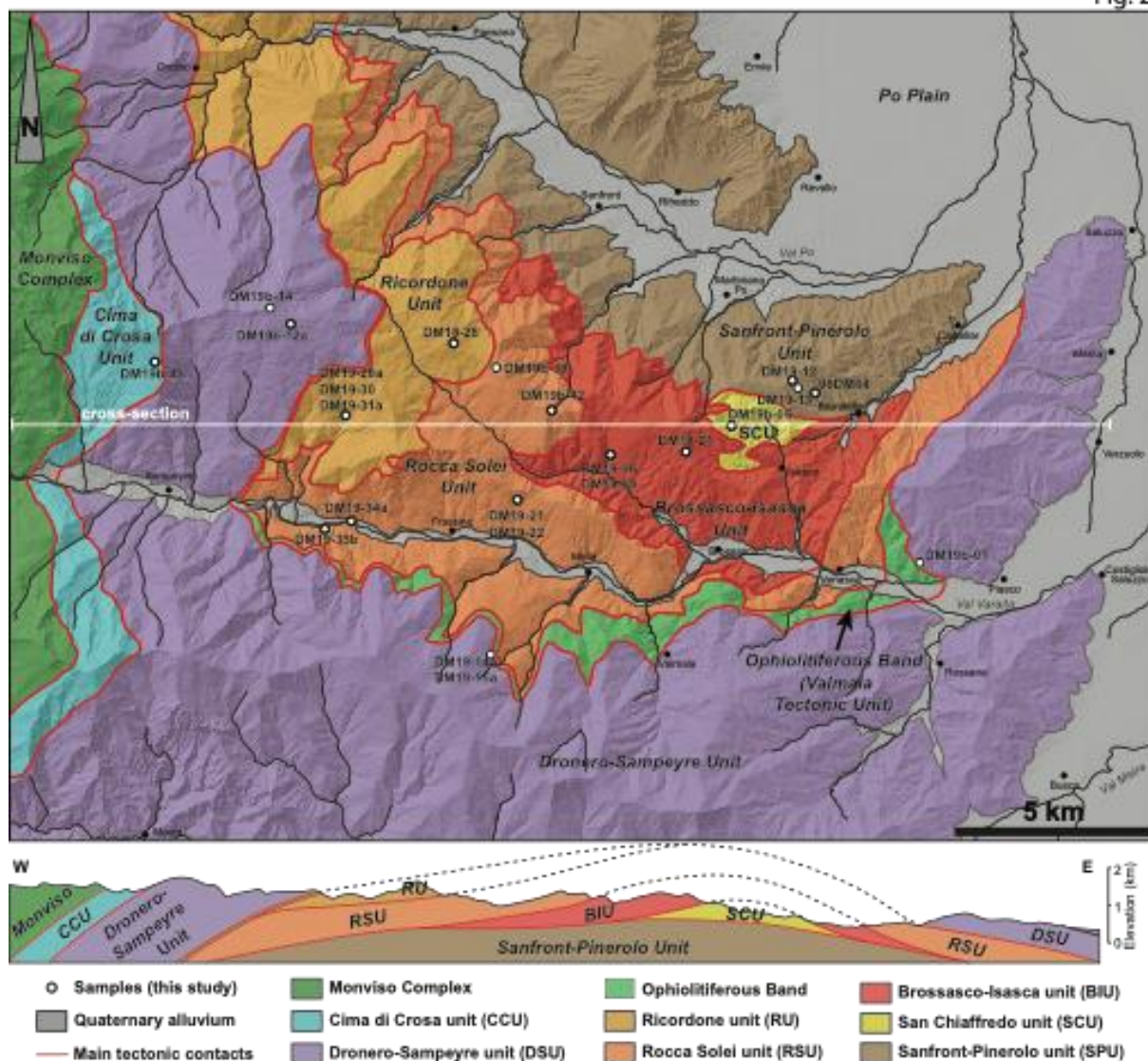
Fig. 2

Fig. 2: Map and cross-section of the units of the southern Dora-Maira massif, around Valle Po and Valle Varaita. Compiled from Malaroda (1972); Kerckhove and Monjuvent (1979); Henry (1990); Chopin et al. (1991); Compagnoni et al. (2012); Groppo et al. (2019); Balestro et al. (2020). The location of the section is shown on the map.

Other units experienced metamorphism at garnet-blueschist-facies to "cold" eclogite-facies conditions, around 2-2.4 GPa and 500-520°C for the Sanfront-Pinerolo, San Chiaffredo, Rocca Solei and Ricordone unit; and upper blueschist-facies conditions of 1.7-1.8 GPa and 450-470°C for the Dronero-Sampeyre unit (Chopin et al., 1991, Avigad et al., 2003; with a recent reexamination by Groppo et al., 2019 for all units). The peak P-T conditions of all units (Fig. 3) are in agreement with the cold metamorphic gradient recorded in the Western Alps (~6-8°C/km, using a lithostatic assumption for pressure to depth conversion; Agard, 2021). These estimates imply a metamorphic gap of at least 1 GPa and 200°C between the hot eclogites of the coesite-bearing unit and the cold eclogites (Fig. 3). No

detailed P-T estimates exist for the Ophiolitiferous band, but Balestro et al. (2020) described garnet-chloritoid assemblages, suggesting P-T conditions close to those of the "cold" eclogite units.

Retrogression affected the whole Dora-Maira massif, with a marked event at ~1.0 GPa and 550°C (Rubatto and Hermann, 2001), whereas the regional foliation parallel to tectonic boundaries was likely acquired during decompression at ~0.5-0.7 GPa and 500-550°C (Chopin et al., 1991; Rubatto and Hermann, 2001; Avigad et al., 2003).

Relics of HT minerals indicate that the Dora-Maira massif experienced several stages of pre-Alpine polymetamorphic evolution, largely overprinted by Alpine HP metamorphism. These stages imply Variscan regional metamorphism at amphibolite-facies conditions, and Late Variscan contact metamorphism (e.g., Vialon, 1966; Chopin et al., 1991; Sandrone et al., 1993; Compagnoni et al., 1995; Compagnoni and Rolfo, 2003; Groppo et al., 2007a; Nosenzo et al., 2022).
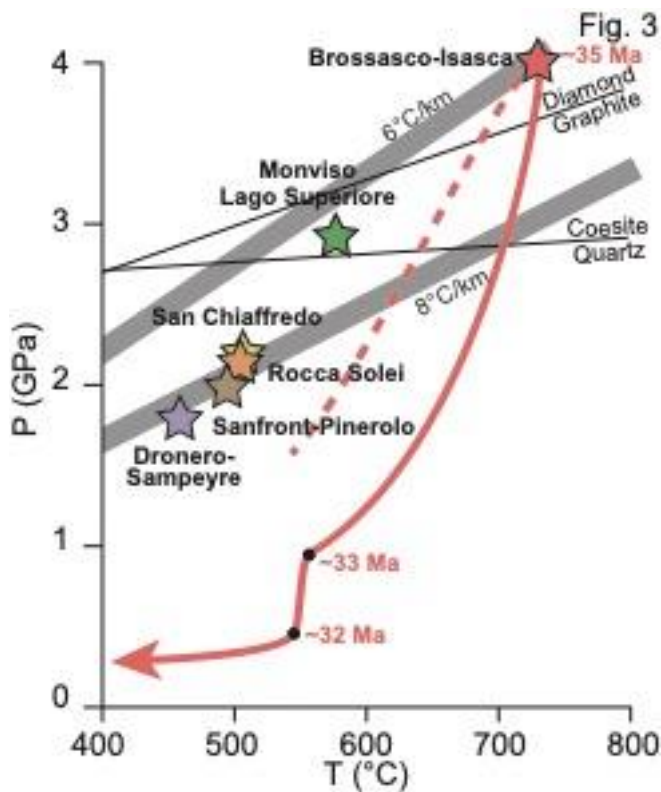
Fig. 3: Compilation of peak P-T conditions (stars) for the units of the southern Dora-Maira massif, P-T-t path for the Brossasco-Isasca UHP unit, after Chopin (1984); Chopin et al. (1991); Rubatto and Hermann (2001); Hermann (2003); Ferrando et al. (2017); Groppo et al. (2019). Peak P-T conditions for the Lago Superiore unit of the Monviso complex are recalled for reference (Locatelli et al., 2018).

1.1. Previous geochronological studies

Geochronology of high-pressure metamorphism in the Dora-Maira massif was initially controversial: the earliest studies interpreted dates around 100-90 Ma as peak metamorphism during an "Eo-alpine" episode with greenschist-facies overprint at ~40 Ma (Vialette and Vialon, 1964; Paquette et al., 1989; Scaillet et al., 1990; Monié and Chopin, 1991). Further studies ascribed those apparent ages to mixed analyses of magmatic cores and metamorphic rims in zircon (Gebauer et al., 1997) or excess argon (Arnaud and Kelley, 1995; Scaillet, 1996). Reliable metamorphic ages obtained in Dora-Maira, other internal crystalline massifs, the Briançonnais and Piemonte-Liguria metaophiolites are summarized on Fig. 1 and Table 1.

Locality	Valley	Unit	Facies	Lithology	Dating method; mineral	Age (Ma)	Event	Ref
Pta Muret	Germanasca	Muret unit	Eclogite	Peraluminous metagranite	U-Pb; zircon	457 ± 2	Mag.	1
Pta Muret	Germanasca	Muret unit	Eclogite	Metagranite	U-Pb; zircon (in-situ)	442 ± 2	Mag.	16
Cavour	Po plain	SPU	Blueschist?	Calc-alkaline metagranite	U-Pb; zircon	304 ± 2	Mag.	1
Malanaggio	Chisone	SPU	Blueschist	Calc-alkaline metadiorite	U-Pb; zircon	290 ± 2	Mag.	1
Malanaggio	Chisone	SPU	Blueschist	Calc-alk. metagranodiorite	U-Pb; zircon	288 ± 2	Mag.	1
Sangone	Sangone	Muret unit	Eclogite	Alkali-calcic metagranite	U-Pb; zircon	279-267	Mag.	1
Freidour	Sangone	SPU	Blueschist	Alkali-calcic metagranite	U-Pb; zircon	283-268	Mag.	1
Parigi	Po	BIU	UHP	Pyrope-whiteschist	U-Pb; zircon	304 ± 2	Mag.	2
Brossasco	Varaita	BIU	UHP	Porphyritic metagranite	U-Pb; zircon	304 ± 3	Mag.	3
Parigi	Po	BIU	UHP	Pyrope-whiteschist	U-Pb; zircon (in-situ)	262 ± 3	Mag.	4
Brossasco	Varaita	BIU	UHP	Metagranite	U-Pb; zircon (in-situ)	262 ± 5	Mag.	5
Brossasco	Varaita	BIU	UHP	Metagranite	U-Pb; zircon (in-situ)	268 ± 6	Mag.	5
Bastoneri	Varaita	BIU	UHP	Metagranite	U-Pb; zircon (in-situ)	267 ± 3	Mag.	5
Bastoneri	Varaita	BIU	UHP	Metagranite	U-Pb; zircon (in-situ)	270 ± 2	Mag.	5
Parigi	Po	BIU	UHP	Whiteschist	U-Pb; zircon (in-situ)	259 ± 6	Mag.	5
Punta Muret	Germanasca	Muret unit	Eclogite	Garnet-staurolite micaschist	U-Pb; monazite (in-situ)	324 ± 6	Amph.	16
Punta Muret	Germanasca	Muret unit	Eclogite	Garnet-staurolite micaschist	U-Pb; zircon (in-situ)	304 ± 2	Amph.	16
Colletto	Chisone	Muret unit	Eclogite	Silvery micaschist	Rb-Sr; white mica	39.5 ± 0.4	Exh.	6
Prato del Colle	Chisone	Muret unit	Eclogite	Silvery micaschist	Rb-Sr; white mica	35.4 ± 2.3	Exh.	6
Val Subiasco	Pellice	Muret unit	Eclogite	Orthogneiss	Ar-Ar; white mica (step-heating)	43.7 ± 0.2	Peak	7
Val Subiasco	Pellice	Muret unit	Eclogite	Orthogneiss	Ar-Ar; white mica (in-situ)	40.3 ± 0.6	Peak	7
Monte Ciarm	Varaita	Up. DSU	Blueschist	Permo-Triassic quartzite	Ar-Ar; white mica (step-heating)	43.7 ± 0.5	Peak	8
Stentivi	Varaita	Low. DSU	Blueschist	Permo-Triassic quartzite	Ar-Ar; white mica (step-heating)	36.8 ± 0.4	Peak	8
Parigi	Po	BIU	UHP	Pyrope-whiteschist	Sm-Nd; garnet	38.5 ± 4.5	Peak	2, 9
Parigi	Po	BIU	UHP	Pyrope-whiteschist	U-Pb; ellenbergerite-pyrope	31.4 ± 1.3	Peak	9
Parigi	Po	BIU	UHP	Pyrope-whiteschist	U-Pb; ellenbergerite-pyrope	35.4 ± 0.3	Peak	9
Parigi	Po	BIU	UHP	Pyrope-whiteschist	U-Pb; monazite-pyrope	34.3 ± 0.3	Peak	9
Parigi	Po	BIU	UHP	Pyrope-whiteschist	U-Pb; monazite-pyrope	34.1 ± 0.7	Peak	9
Parigi	Po	BIU	UHP	Pyrope-whiteschist	Lu-Hf; garnet; recalculated	34.1 ± 1.0	Peak	10
Parigi	Po	BIU	UHP	Pyrope-whiteschist	U-Pb; zircon (in-situ)	34.6 ± 0.7	Peak	11
Parigi	Po	BIU	UHP	Pyrope-whiteschist	U-Pb; zircon (in-situ)	34.9 ± 0.3	Peak	12
Parigi	Po	BIU	UHP	Pyrope-whiteschist	U-Pb; zircon (in-situ)	35.1 ± 0.5	Peak	12
Parigi	Po	BIU	UHP	Pyrope-whiteschist	U-Pb; zircon (in-situ)	34.6 ± 0.7	Peak	12
Parigi	Po	BIU	UHP	Pyrope-whiteschist	U-Pb; monazite (in-situ)	34.7 ± 0.4	Peak	12
Parigi	Po	BIU	UHP	Pyrope-whiteschist	U-Pb; zircon (in-situ)	34.1 ± 0.3	Peak	4
Parigi	Po	BIU	UHP	Pyrope-whiteschist	U-Pb; zircon (in-situ)	35.0 ± 1.4	Peak	5
Parigi	Po	BIU	UHP	Pyrope-whiteschist	U-Pb; zircon (in-situ)	34.4 ± 1.1	Peak	5
Parigi	Po	BIU	UHP	Jadeite-quartzite	U-Pb; zircon (in-situ)	34.2 ± 0.7	Peak	13
Parigi	Po	BIU	UHP	Orthogneiss	U-Pb; zircon (in-situ)	34.7 ± 0.3	Peak	13
Garneri	Varaita	BIU	UHP	Mafic eclogite	Rb-Sr; white mica	36.3 ± 1.9	Peak	14
Costa Monforte	Varaita	BIU	UHP	Calcsilicate rock	U-Pb; titanite (in-situ)	35.1 ± 0.9	Peak	15
Costa Monforte	Varaita	BIU	UHP	Calcsilicate rock	U-Pb; titanite (in-situ)	32.9 ± 0.9	Exh.	15
Costa Monforte	Varaita	BIU	UHP	Calcsilicate rock	U-Pb; titanite (in-situ)	31.8 ± 0.5	Exh.	15

Table 1: Synthesis of previous geochronological studies in the Dora-Maira massif. The Muret unit (mostly polymetamorphic) is generally considered as a lateral equivalent of the Ricordone or Rocca Solei unit. Abbreviations: SPU, Sanfront-Pinerolo unit; BIU, Brossasco-Isasca unit; UHP, ultra-high pressure; Mag., magmatism; Amph., amphibolite-facies metamorphism; Exh., exhumation. References: 1, Bussy and Cadoppi (1996); 2, Tilton et al. (1989); 3, Paquette et al. (1999); 4, Chen et al. (2016); 5, Chen et al. (2017); 6, Angiboust and Glodny (2020); 7, Scaillet et al. (1990); 8, Monié and Chopin (1991); 9, Tilton et al. (1991); 10, Duchêne et al. (1997); 11, Gebauer et al. (1997); 12, Gauthier-Putallaz et al. (2016); 13, Xiong et al. (2021); 14, Di Vincenzo et al. (2006); 15, Rubatto and Hermann (2001); 16, Nosenzo et al. (2022). A significant number of Ar-Ar dates affected by excess argon were dismissed.

Pyrope whiteschists of the Brossasco-Isasca unit have been extensively studied with different isotopic systems that have yielded consistent ages of peak UHP metamorphism. Early analyses by Tilton et al. (1989, 1991) yielded dates of 35.4 ± 2 Ma and 31.4 ± 1.3 Ma (U-Pb ellenbergerite-pyrope isochrons), 34.3 ± 0.3 Ma and 34.1 ± 0.7 Ma (U-Pb monazite-pyrope isochrons), ~38 Ma (U-Pb zircon isochrons) and 38.5 ± 4.5 Ma (Sm-Nd pyrope isochron). This ~35-34 Ma age for peak metamorphism has been confirmed by a substantial amount of zircon dates, at 34.6 ± 0.7 Ma (concordant SHRIMP analyses, recalculated weighted mean of the least discordant zircons, Gebauer et al., 1997), 35.1 ± 0.5 Ma (zircon core), 34.9 ± 0.3 Ma, 35.1 ± 0.8 Ma (zircon rims, SHRIMP, Gauthiez-Putallaz et al., 2016) and by analyses of zircon rims at 34.1 ± 0.3 Ma, 36.5 ± 0.6 Ma, 40.2 ± 0.6 Ma (SIMS, Chen et al., 2016), 35.0 ± 1.4 Ma and 34.4 ± 1.1 Ma (ICP-MS, Chen et al., 2017), 34.2 ± 0.7 Ma (SIMS, Xiong et al., 2021). Monazite U-Pb dating yielded dates of 34.7 ± 0.4 Ma (SHRIMP, Gauthiez-Putallaz et al., 2016). Pyrope-whole rock Lu-Hf geochronology yielded a date of 32.8 ± 1.2 Ma (Duchêne et al., 1997, recalculated to 34.1 ± 1.0 Ma with the ^{176}Lu decay constant of Söderlund et al., 2004).

Similar ages of peak metamorphism have been obtained in other rock types from the Brossasco-Isasca UHP unit. Rubatto and Hermann (2001) obtained a similar age for peak metamorphism with titanite U-Pb isochrons in calc-silicate rocks at 35.1 ± 1.8 Ma, and obtained 32.9 ± 1.8 Ma and 31.8 ± 1.0 Ma ages for retrogression at greenschist-facies conditions. Rb-Sr omphacite-phengite-whole rock dating yielded an isochron date of 36.3 ± 0.3 Ma in a mafic eclogite of the same unit (Di Vincenzo et al., 2006). SIMS dating of coesite-bearing zircon rims from the country orthogneiss reflected a metamorphic age of 34.7 ± 0.3 Ma (Xiong et al., 2021).

Few studies focused on the metamorphic ages of the other units (mostly Ar-Ar geochronology, usually affected by excess argon). Notably, Scaillet et al. (1990) obtained a "reliable age of ~40 Ma for retrogressive deformation" in one of the upper units of Dora-Maira in Val Pellice and Monié and Chopin (1991) obtained Ar-Ar dates of 43.7 ± 0.5 Ma and 36.8 ± 0.4 Ma on white micas from monometamorphic metasediments (Permo-Triassic quartzites) of the Dronero-Sampeyre unit.

A number of inherited ages have also been reported in the literature: Caledonian (457 ± 2 Ma, 442 ± 2 Ma) and late Variscan (mainly Permian ~304 Ma, 304 ± 3 Ma, 290 ± 2 Ma, 288 ± 2 Ma, 283-268 Ma, 280-267 Ma and 268 ± 5 Ma) magmatic ages have been reported for orthogneisses and metagranites throughout the massif (Tilton et al., 1989; Bussy and Cadopi, 1996; Paquette et al., 1999; Xiong et al., 2021, Nosenzo et al., 2022). In pyrope whiteschists, Tilton et al. (1989) defined a zircon U-Pb isochron upper intercept at 304 ± 2 Ma, whereas Gebauer et al. (1997) showed that oscillatory-zoned zircons record magmatic ages as old as ~275 Ma (isochron upper intercept). The most recent dates of zircon cores define a slightly younger protolith age of the whiteschists consistent with magmatic ages of the orthogneiss at 262 ± 3 Ma, 261 ± 9 Ma and 261 ± 7 Ma, 259 ± 6 Ma (Gauthiez-Putallaz et al., 2016;

Chen et al., 2017; Xiong et al., 2021). The peak of pre-Alpine amphibolite-facies metamorphism was dated at 324 ± 6 Ma in the Punta Muret unit (northern Dora-Maira massif), with a subsequent (greenschist-facies?) metamorphic event at 304 ± 2 Ma (Nosenzo et al., 2022).

Detrital or metamorphic titanites as old as 253 Ma were found in the calcsilicates of the coesite-bearing unit (Rubatto and Hermann, 2001). In Sanfront-Pinerolo unit metasediments, the youngest detrital zircons have Carboniferous ages of 330 Ma (Manzotti et al., 2016), while this method yielded Ediacarian and Ordovician sedimentation ages (598 ± 2 Ma, 453 ± 4 Ma) in the Muret unit (Nosenzo et al., 2022).

2. Structural context and sampling strategy

For this study, several maps of the area were compiled, in particular Vialon (1966), Malaroda (1972), Henry (1990), Henry et al. (1993), Compagnoni et al. (2012), Groppo et al. (2019), and Balestro et al. (2020). This led to the map presented in Fig 2. Tectonic contacts within the main basement domain of Dora-Maira (San Chiaffredo, Brossasco-Isasca, Rocca Solei and Ricordone units) are locally marked by thin Mesozoic (meta)sedimentary successions intercalated between orthogneiss exposures (well visible on the crest north of Vallone Gilba). In most areas, outcrop quality is poor, and many contacts are interpolated. In order to have a representative sampling of high-pressure metamorphic assemblages and maximize chances to find datable rutile and titanite, samples were collected from various lithologies in all units. Attention was given to sampling metasediments expected to be more reactive, in particular impure quartzites and marbles likely corresponding to lithologies observed in the Triassic Briançonnais domain (i.e. monometamorphic), but also ankerite and organic-matter-rich metasediments of assumed Carboniferous-Permian age. Other metasedimentary rocks may include older protoliths like schists and carbonate intercalations of the polymetamorphic basement. We also sampled pyrope-bearing whiteschists in the Brossasco-Isasca unit and mafic eclogites found as lenses in orthogneiss. Macroscopic field features are shown on Supporting Figure S1.

3. Sample description, from the field to the microscope

Twenty-four samples have been collected in a variety of lithologies along an east-west transect at latitudes between 44°32' and 44°39' in the Varaita and Po valleys. Samples are located on the map of Fig. 2.
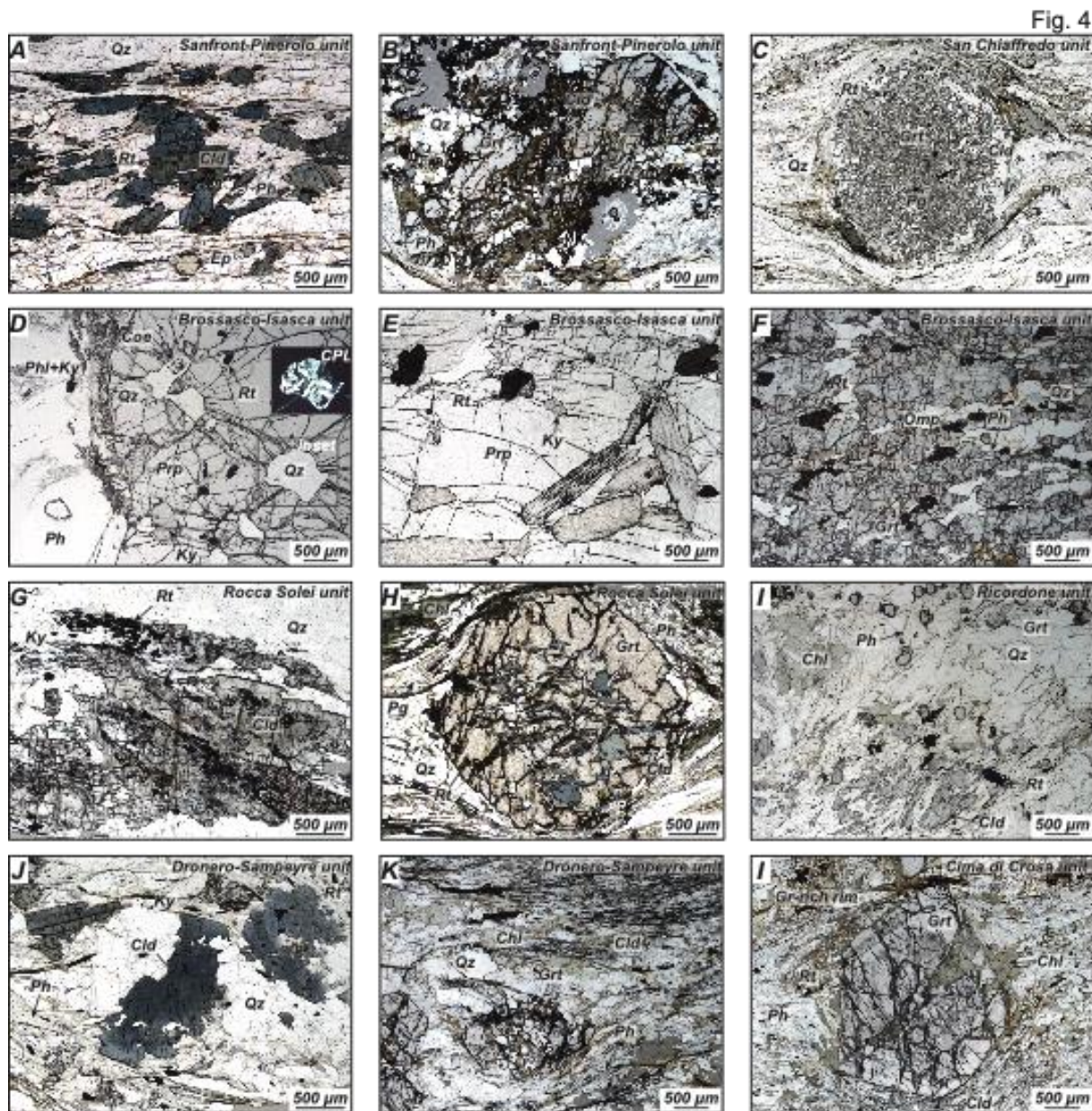
Fig. 4: Petrography of selected samples showing eclogite-facies assemblages in all units, and textural association of rutile with high-pressure minerals. A- Rutile inclusions in chloritoid in a micaschist from the Sanfront-Pinerolo unit (DM19-12). B- Garnet porphyroblast with quartz and chloritoid inclusions in a micaschist from the Sanfront-Pinerolo unit (DM19-13). C- Garnet porphyroblast with paragonite, chloritoid and rutile inclusions from the San Chiaffredo unit (DM19b-05). D- Rutile, coesite and kyanite inclusions in the same textural domains of a garnet crystal in a pyrope-whiteschist from the Brossasco-Isasca unit. Inset shows palisade textures of quartz inclusions in cross-polarized light (DM19-06). E- Rutile and kyanite inclusions in pyrope megablast from the Brossasco-Isasca unit (DM19-09). F- Textural equilibrium between garnet, omphacite, rutile, phengite and quartz in a mafic eclogite from the Brossasco-Isasca unit (DM18-21). G- Association of rutile with kyanite and chloritoid in a micaschist from the Rocca Solei unit (DM19-22). H- Chloritoid and rutile inclusions in garnet in a micaschist from

the Rocca Solei unit (DM19b-42). I- Rutile association with garnet and chloritoid in a micaschist from Ricordone unit (DM18-28). J- Rutile association with kyanite and chloritoid in a micaschist from the Dronero-Sampeyre unit (DM19b-12a). K- Coexistence of garnet and chloritoid in a micaschist from the Dronero-Sampeyre unit (DM19b-01). L- Rutile inclusions in a garnet rim, itself at equilibrium with chloritoid from the Cima di Crosa unit (DM19b-43). Abbreviations: Amp, amphibole; Cb, carbonate; Chl, chlorite; Cld, chloritoid; Coe, coesite; Ep, epidote; Gr, graphite; Grt, garnet; Ky, kyanite; Pg, paragonite; Ph, phengite; Phl, phlogopite; Prp, pyrope; Qz, quartz; Rt, rutile.

Sanfront-Pinerolo unit

98DM64 is a metamarl. An assemblage of epidote, quartz, ankerite, amphibole and submillimetric titanite is observed, partially retrogressed into chlorite.

DM19-12 is a chloritoid micaschist. Chloritoid, quartz, white mica, ankerite and rutile are part of the peak assemblage, in which rutile occurs as <50 μm inclusions within chloritoid (Fig. 4A). Chlorite, in shear bands, and ilmenite around rutile are part of the retrograde assemblage. DM19-13 is a garnet-chloritoid micaschist. Peak metamorphic assemblages of some domains contain garnet with rotated inclusions of chloritoid, clinozoisite (possibly pseudomorph after lawsonite) and rutile in a quartz, ankerite and white mica foliated matrix (Fig. 4B), while other domains contain mostly foliated white mica and chloritoid. Rutile occurs as <100 μm inclusions in garnet and chloritoid. Retrograde assemblages consist of chlorite in garnet cracks and after white mica, and ilmenite around rutile.

San Chiaffredo unit

DM19b-05 is a garnet micaschist. The peak metamorphic assemblage consists of garnet porphyroblasts, with inclusions of quartz, white mica, clinozoisite (likely former lawsonite) and rutile, in a quartz and white mica and rutile foliated matrix (Fig. 4C). Rutile occurs as <200 μm-long aligned inclusions in centimeter-sized garnet and in the matrix foliation. The retrograde assemblage consists of chlorite around garnet and in shear bands, and ilmenite around rutile.

Brossasco-Isasca unit

DM19-06 (Fig. 4D) is a pyrope-quartzite with ~1 cm-large garnet crystals with fresh coesite inclusions ("porphyroblast", according to the classification by Ferrando et al., 2009). Other peak minerals include kyanite and ~150 μm-large rutile inclusions in garnet, and phengite, kyanite, (up to 720x400 μm) rutile in a silica matrix (former coesite), rutile. Limited retrogression is marked by thin phlogopite-kyanite symplectites around garnet (a detailed petrographic description of these rocks is given by Chopin, 1984).

DM19-09 (Fig. 4E) is a pluricentimetric garnet from a pyrope-quartzite ("megablast", according to the classification by Ferrando et al., 2009). Inclusions of kyanite, jadeite, white mica and <200 µm-large rutile crystals are all characteristic of peak metamorphism. No retrogression phases are observed in the sample.

DM18-21 (Fig. 4F) is a foliated mafic eclogite. The peak metamorphic assemblage consists of garnet, omphacite, submillimetric rutile, white mica and silica (former coesite). Retrogression is marked by glaucophane in pressure shadows of garnet and omphacite, and thin symplectites around garnet and white mica. This sample is comparable to the one studied by Groppo et al. (2007b).

Rocca Solei unit

DM19-21 is a garnet micaschist. The peak assemblage is composed of garnet, white mica, clinozoisite (with allanite core), ~100 µm rutile and quartz. Retrogression is marked by chlorite crystallization after garnet and white mica and ilmenite after rutile.

DM19-22 is a chloritoid micaschist. The peak assemblage consists of kyanite, chloritoid, white mica, rutile graphite and quartz. Rutile occurs in graphite-rich domains as <100 µm long crystals, commonly included in kyanite and chloritoid (Fig. 4G). Retrogression is marked by minor replacement of chloritoid by chlorite.

DM19-33b is a foliated impure marble. The peak metamorphic assemblage consists of carbonate, phengite and ~370x250 µm rutile, while the retrograde assemblage consists of titanite around or replacing rutile, chlorite and clinozoisite. Rutile occurs either as crystals equilibrated with calcite or as smaller, <100 µm long crystals in the foliation with white mica and chlorite.

DM19-34a1 is a mafic eclogite, intercalated with pure marble at the decimeter scale. The peak metamorphic assemblage of the rock consists of garnet, omphacite, and ~500x180 µm rutile inclusions in omphacite. Retrograde phases include titanite around rutile, blue-green amphibole, clinozoisite and white mica.

DM19b-39 is a micaschist. The peak metamorphic assemblage consists of foliated white mica, quartz, epidote and <50 µm-large rutile crystals. Retrogression is marked by partial replacement of mica by chlorite, and the occurrence of albite, possibly after jadeite or glaucophane.

DM19b-42 (Fig. 4H) is a garnet-chloritoid micaschist. Garnet, chloritoid (as oriented inclusions in garnet and in the foliated matrix), white mica, epidote, tourmaline, quartz, and ~100 µm-long rutile crystals (included in garnet, chloritoid, epidote, and in the matrix) are part of the peak assemblage. Retrograde phases consist of chlorite after white mica and ilmenite after rutile.

Ricordone unit

DM18-28 (Fig. 4I) is a garnet-chloritoid micaschist. Peak minerals are garnet, chloritoid, submillimetric rutile (texturally associated to chloritoid), white mica, glaucophane, and quartz. Retrograde minerals are ilmenite after rutile, chlorite after chloritoid and white mica, and albite and chlorite after glaucophane.

DM19-28a is a garnet micaschist. The peak metamorphic assemblage consists of garnet, white mica, tourmaline, quartz, and < 100 µm rutile crystals in the foliation. Retrogression is marked by chlorite after garnet and white mica, and ilmenite around or completely replacing rutile.

DM19-30 is a garnet micaschist. Garnet with large (> 100 µm) oriented inclusions of quartz and rutile occurs in a matrix composed of white mica, epidote, rutile (~50 µm crystals) and quartz. Retrograde minerals are chlorite after garnet and white mica, and titanite around rutile.

DM19-31a is a garnet micaschist. Two generations of garnet are observed: one with large (> 100 µm) elongated and oriented quartz inclusions, the second one with ilmenite inclusion in the cores and 100-150 µm rutile inclusions in the rims. They are surrounded by a matrix composed of quartz, white mica, chloritoid, and 150-300 µm rutile. Retrogression is marked by chlorite in the matrix and in garnet cracks and titanite around rutile.

Dronero-Sampeyre unit

DM19-14a is a chloritoid-kyanite quartzite. The peak mineral assemblage consists of quartz, kyanite, chloritoid, minor white mica and carbonate and <100 µm rutile crystals (included in kyanite and chloritoid and in the quartz matrix). The sample is almost unaffected by retrogression.

DM19-15a is a chloritoid micaschist. Peak minerals are chloritoid, white mica, graphite (within lawsonite pseudomorphs), quartz, and rutile. Rutile occurs in graphite-rich domains as 100-400 µm-long crystals in the foliation, occasionally rimming chloritoid. The sample is almost unaffected by retrogression.

DM19b-01 is a garnet micaschist. The peak mineral assemblage consists of garnet, in a matrix of white mica, chloritoid, tourmaline, quartz and <100 µm rutile crystals (a few are included in garnet) It is one of the rare samples where garnet and chloritoid are both present (although in distinct domains, Fig. 4K – though chloritoid is occasionally found as inclusions in garnet in other samples). Retrogression is characterized by chlorite in garnet cracks and after white mica, and ilmenite around or completely replacing rutile.

DM19b-12a (Fig. 4J) is a chloritoid micaschist. The peak mineral assemblage consists of chloritoid, kyanite, epidote, white mica, quartz, and rutile, the latter occurring as <100 µm-long crystals, as inclusions within chloritoid and in the white mica foliation. Retrogression is marked by the occurrence of >100 µm ilmenite (locally surrounding rutile), and chlorite (after chloritoid and white mica).

DM19b-14 is a calcschist. The peak mineral assemblage consists of carbonate, chloritoid, quartz, white mica, epidote, apatite, and <100 μm rutile crystals (in the matrix and as inclusions within chloritoid) Retrogression is marked by chlorite after white mica and chloritoid, and titanite around rutile.

Cima di Crosa unit

DM19b-43 (Fig. 4L) is a garnet micaschist. The peak metamorphic assemblage consists of garnet porphyroblasts (up to 5 mm large), with chloritoid, graphite and <200 μm-long rutile inclusions in the rim, as well as white mica, rutile (of similar size as inclusions), tourmaline and quartz in a foliated matrix. Retrogression is marked by ilmenite after rutile in the matrix, rhombic pseudomorphs of albite and chlorite (likely after glaucophane) and chlorite after white mica and garnet.

4. Materials and methods

4.1. U-Pb isotopes and trace elements analysis

Titanite and rutile were analyzed by LASS (laser ablation split-stream) at the University of California, Santa Barbara, following the method of Garber et al. (2017); after ablation, the U-Pb isotopes and trace elements were analyzed simultaneously on a multicollector and a quadrupole mass spectrometer. Samples were ablated using a Photon Machine 193nm ArF ultraviolet laser with a HelEx ablation cell, coupled to an Agilent 7700X quadrupole ICP-MS system for trace element measurements and a Plasma 3D or Plasma HR-ES multicollector ICP-MS for U-Pb measurements. We systematically used a 35 μm spot size and a laser fluence of ~1 J.cm^{-2}. Pre-ablation shots were fired on the samples at 50% laser power to remove surface contamination, and the material was allowed to wash out for ~15 s. Material was then ablated at 4Hz during ~25 s. Analyses of unknowns were bracketed by analyses of matrix-matched reference materials MKED (1517.3 ± 0.3 Ma ^{238}U/^{206}Pb date; Spandler et al., 2016) for titanite and Kragerø (~1090 Ma ID-TIMS date; Luvizotto et al., 2009; Bracciali et al., 2013) for rutile.

Secondary U-Pb standards were included in each run as a monitor of accuracy. During the course of this study, we obtained common-Pb corrected (Stacey-Kramers iterative correction in IsoplotR after Stacey and Kramers, 1975; Vermeesch, 2018) dates of 1043.6 ± 3.2 Ma (n = 71) for BLR (1047.1 ± 1.4 Ma Concordia date; Aleinikoff et al., 2007), 391.9 ± 1.6 Ma (n = 47) for Y1710C5 (388.6 ± 0.5 Ma TIMS date; Spencer et al., 2013), 28.7 ± 0.02 Ma (n = 46) for FC titanite (28.4 ± 0.05 MA TIMS date; Schmitz and Bowring, 2001) and 393.9 ± 1.2 Ma (n = 128), for R9826J (381.9 ± 1.1 Ma TIMS date; Kylander-Clark et al., 2008), 2834.0 ± 9.4 Ma (n = 78) for Wodgina (2845.4 ± 0.5 Ma Tera-Wasserburg Concordia date; Ewing, 2011), for rutile. These dates are accurate to within 0.4% (BLR), 0.8% (Y1710C5), 1.0% (FC), 3.1% (R9826J, but analysis of different grains yielded different dates, within 1.1% for one grain

and 5.6% for another grain, suggesting within-sample heterogeneity), and 0.04% (Wodgina) of the reference values.

All unknowns were additionally bracketed by analyses of glass standards NIST SRM 610 (Jochum et al., 2011) or BHVO-2G (Jochum et al., 2005) that were used as primary reference materials for trace elements in titanite and rutile, respectively. Measured peaks were ^{29}Si, ^{44}Ca, ^{49}Ti, ^{51}V, ^{52}Cr, ^{56}Fe, ^{89}Y, ^{90}Zr, ^{93}Nb, ^{178}Hf, ^{181}Ta, ^{139}La, ^{140}Ce, ^{141}Pr, ^{146}Nd, ^{147}Sm, ^{153}Eu, ^{157}Gd, ^{159}Tb, ^{163}Dy, ^{165}Ho, ^{166}Er, ^{169}Tm, ^{172}Yb, ^{175}Lu, ^{178}Hf, ^{181}Ta for titanite, and ^{28}Si, ^{44}Ca, ^{49}Ti, ^{31}P, ^{45}Sc, ^{51}V, ^{52}Cr, ^{56}Fe, ^{89}Y, ^{90}Zr, ^{93}Nb, ^{182}W for rutile. Internal standardization of trace elements was done on Ca for titanite (assuming 19.25 wt.% Ca), and Ti for rutile (assuming 59.94 wt.% Ti).

The Iolite plug-in (Paton et al., 2011) for the Wavemetrics Igor Pro Software was used to correct measured isotopic ratios for baselines, time-dependent laser-induced fractionation, and instrument drift. Baseline intensities were determined prior to each analysis. Uncertainties on isotopic measurements were extracted from Iolite. The error correlation between the ^{238}U/^{206}Pb and ^{207}Pb/^{206}Pb ratios was recalculated following the method of Schmitz and Schoene (2007). A quadratic uncertainty was added to isotopic ratios to account for analytical uncertainty so that the MSWD of the weighted means of ^{238}U/^{206}Pb and ^{207}Pb/^{206}Pb equals to 1 for secondary reference materials BLR (titanite) or R9826J (rutile) for each run. This correction adds relative uncertainties of 1.5-10% (for ^{238}U/^{206}Pb) and 0.9-2.5% (for ^{207}Pb/^{206}Pb) on the ratios.

In all calculations, spots with values of Zr, P or Si inconsistent with rutile/titanite analyses were not considered in date calculation in order to avoid the contamination by inclusions of zircon, apatite/monazite/xenotime, or allanite, respectively, which are common minerals in Dora-Maira rocks. Calcium, potentially affected by titanite, was additionally monitored in rutile, as well as Ti in titanite (affected by rutile). Samples with particularly unradiogenic rutile and titanite were not considered for geochronology.

Analyses were sorted to extract populations with homogeneous trace-element patterns, and isochron dates were calculated from the Tera-Wasserburg projection using the "spine" robust regression by Powell et al. (2020). Contrary to the traditional least-squares regression by York (1967), this method does not assume a Gaussian uncertainty on the scatter of the individual analyses, and hence is less sensitive to outliers. This method optimizes error calculation, and yields isochrons (with errors) when spines pass a 95% confidence test, and less probable errorchrons (without errors) when they fail the test. A detailed study of the significance of rutile U-Pb dates (in function of grain size and peak metamorphic temperatures) is presented in the discussion and in Supporting Figures S4 and S5.

4.2. Temperature estimates

Zirconium concentrations in rutile from Zr-buffered assemblages may be temperature dependent (Zack et al., 2002; Zack et al., 2004). In this study, we tested two calibrations of the thermometer: the pressure-dependent experimental calibration of Tomkins et al. (2007), and the Kohn (2020) expression combining natural and experimental data. The Kohn (2020) calibration yields temperatures lower than the former expression at low temperature (up to 40°C at low temperature, Table 2), and the results presented here are closer to temperatures expected from mineral assemblages and thermodynamic modeling. The activity of $ZrSiO_4$ was set to unity, because zircon occurs in most samples. The calibration in the α-quartz stability field was used for rocks in the non-UHP units, whereas temperatures in the UHP unit were determined with the calibration in the coesite stability field. Pressures determined by Groppo et al. (2019) were used for calculation (2.0 GPa for prograde metamorphism in the Rocca Solei unit, and peak pressures of 4.0 GPa for the Brossasco-Isasca unit, 2.2 GPa for peak in the Sanfront-Pinerolo, San-Chiaffredo, Rocca Solei, and Ricordone units, 1.7 GPa for the Dronero-Sampeyre unit). A pressure of 2.0 GPa was attributed to the Cima di Crosa unit, consistent with eclogite-facies assemblages.

Temperature was also estimated for titanite crystallization, using the thermometer of Hayden et al. (2008). Silica and titania activity were set to unity, and pressure was set between 0.3 and 0.5 GPa depending on samples. A summary of pressures used for temperature calculations is shown in Table 2.

5. Results

5.1. Zr-in-rutile and Zr-in-titanite thermometry

Results of Zr-in-rutile thermometry are shown on Fig. 5 and Table 2. Hereafter temperature estimates are from Kohn (2020), and values in parenthesis are from Tomkins et al. (2007). Uncertainties are given as 2σ. Results for other trace elements are not detailed, they are mostly linked to the lithology (in particular Nb).
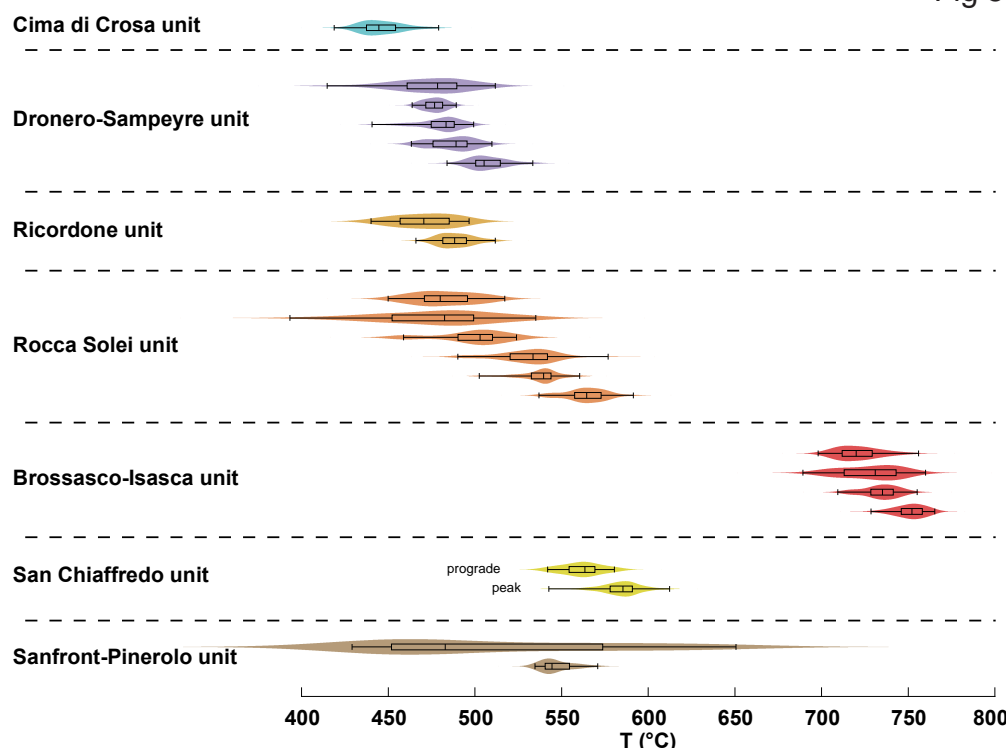
Fig. 5: Synthesis of Zr-in-rutile thermometry results (from Tomkins et al., 2007, shown as violin plots, consisting of a box plot wit minimum, first quartile, median, third quartile and maximum values, superimposed with a kernel density plot of the temperatures). Peak temperatures around 400°C are recorded for the Cima di Crosa unit, 450-500°C for the Dronero-Sampeyre and Ricordone units, 450-550°C for the Rocca Solei unit, 700-750°C for the Brossasco-Isasca unit, ~550°C for the San Chiaffredo unit and 500-550°C for the Sanfront-Pinerolo unit.

Sanfront-Pinerolo unit

Rutile in DM19-12 records a wide temperature range, averaging at 474 ± 152°C (513 ± 144°C, n = 38), while in sample DM19-13, the temperature range is more restricted at 513 ± 20°C (551 ± 19°C, n = 26)

San Chiaffredo unit

Rutile inclusions in garnet from sample DM19b-05 record temperatures of 524 ± 24°C (562 ± 22°C, n = 21), while matrix rutile records an average temperature of 549 ± 24°C (584 ± 23°C, n = 98).

Brossasco-Isasca unit

Rutile from mafic eclogite DM18-21 yields a peak temperature of 701 ± 28°C (721 ± 25°C, n = 100). Rutile in pyrope whiteschists samples DM19-06 and DM19-09 records peak temperatures of 713 ± 30°C (732 ± 27°C, n = 114) and 734 ± 19°C (751 ± 17°C, n = 62), respectively.

Rocca Solei unit

Rutile from mafic sample DM19-34a1 records a peak temperature of 531 ± 25°C (567 ± 23°C, n = 58). Rutile from garnet-micaschist samples DM19b-42 and DM19-21 yields temperatures of 499 ± 25°C (527 ± 23°C, n = 35) and 495 ± 42°C (534 ± 34°C, n = 61), respectively. Rutile from garnet-free micaschists DM19b-39 and DM19-22 yields lower average temperatures of 436 ± 70°C (478 ± 67°C, n = 41) and 441 ± 36°C (483 ± 35°C, n = 79). Rutile in the foliation of sample DM19-33b (impure marble) yields average temperatures of 461 ± 42°C (502 ± 41°C, n = 41).

Unit	Sample	Mineral	Age	2σ	$^{207}Pb/^{206}Pb_0$	2σ	n	s	slim	P (GPa)	T_{Kohn}	2σ	$T_{Tomkins}$	2σ	T_{Hayden}	2σ
SPU	98DM64	Titanite	291	-	0.829	-	42	2.21	1.28	0.3	-	-	-	-	656	46
SPU	DM19-12	Rutile	32.7	2.2	0.843	0.004	38	1.06	1.29	2.2	474	152	513	144	-	-
SPU	DM19-13	Rutile	-	-	-	-	26	-	-	2.2	513	20	551	19	-	-
SCU	DM19b-05 inclusions	Rutile	35	3.5	0.831	0.006	21	1.19	1.36	2.0	524	24	562	22	-	-
SCU	DM19b-05 matrix	Rutile	33.3	4.5	0.821	0.005	98	1.1	1.16	2.2	549	24	584	23	-	-
BIU	DM18-21	Rutile	31.6	-	0.823	-	100	1.5	1.16	4.0	701	28	721	25	-	-
BIU	DM19-06 inclusions	Rutile	33.1	-	0.729	-	59	1.33	1.23	4.0	689	37	704	33	-	-
BIU	DM19-06 matrix	Rutile	37.4	3.3	0.724	0.04	43	1.1	1.28	4.0	696	22	710	20	-	-
BIU	DM19-09	Rutile	34	-	0.823	-	62	1.47	1.23	4.0	734	19	751	17	-	-
RSU	DM19-21	Rutile	-	-	-	-	61	-	-	2.2	495	42	534	34	-	-
RSU	DM19-22	Rutile	35.9	3.1	0.825	0.002	79	1.12	1.19	2.2	441	36	483	35	-	-
RSU	DM19-33b	Titanite	31.2	-	0.783	-	41	1.71	1.28	0.5	-	-	-	-	571	54
RSU	DM19-34a1	Rutile	-	-	-	-	58	-	-	2.2	531	25	567	23	-	-
RSU	DM19b-39	Rutile	-	-	-	-	41	-	-	2.2	436	70	478	67	-	-
RSU	DM19b-42	Rutile	36.3	3.3	0.803	0.007	35	1.16	1.3	2.2	499	25	527	23	-	-
RSU	DM19-34c	Titanite	238	32.2	0.869	0.012	40	0.99	1.29	0.3	-	-	-	-	644	14
RU	DM18-28	Rutile	40.1	6.9	0.841	0.003	60	1.23	1.23	2.2	448	20	489	20	-	-
RU	DM19-28a	Rutile	-	-	-	-	57	-	-	2.2	433	34	475	32	-	-
RU	DM19-30	Rutile	356	35.4	0.858	0.016	21	0.9	1.36	0.6	531	22	545	18	-	-
RU	DM19-31a matrix	Rutile	323	-	0.76	-	40	2.04	1.29	0.6	559	18	569	16	-	-
RU	DM19-31a inclusions	Rutile	293	-	0.903	-	51	2.44	1.25	0.3	509	24	525	20	-	-
DSU	DM19-14a	Rutile	-	-	-	-	29	-	-	1.7	438	25	482	24	-	-
DSU	DM19-15a	Rutile	37.7	2.8	0.829	0.013	60	1.07	1.23	1.7	445	22	477	12	-	-
DSU	DM19b-01	Rutile	-	-	-	-	39	-	-	1.7	426	44	470	42	-	-
DSU	DM19b-12a	Rutile	37.3	0.8	0.822	0.007	57	1.16	1.24	1.7	433	13	507	21	-	-
DSU	DM19b-14	Rutile	-	-	-	-	51	-	-	1.7	431	26	475	25	-	-
CCU	DM19b-43	Rutile	39.8	3.8	0.824	0.003	88	1.05	1.18	2.2	415	26	443	24	-	-

Table 2: Synthesis of rutile and titanite U-Pb geochronology and Zr-in-rutile thermometry. Isochrons are defined by s ≤ slim, and errorchrons by s > slim, where s is the spine width, and slim the 95% confidence limit on spine width to define an isochron (Powell et al., 2020). $^{207}Pb/^{206}Pb_0$ is the Pb composition of the upper intercept of the Tera-Wasserburg diagram (common-Pb composition). n is the number of spots. P(GPa) represents the assumed pressure of crystallization used for thermometry. All uncertainties are given as 2σ. Uncertainties on temperatures are derived from the scatter of temperature of all spots. Temperatures using the calibration of Kohn (2020) and Tomkins (2007) for rutile are compared. Temperatures for titanite are calculated using the calibration of Hayden et al. (2008). Isochrons of samples with inherited rutile and titanite are shown on Supporting Figure S3.

Ricordone unit

Rutile from micaschist samples DM18-28 and DM19-28a yields peak temperatures of 448 ± 20°C (489 ± 20°C, n = 60) and 433 ± 34°C (475 ± 32°C, n = 57), respectively.

Dronero-Sampeyre unit

Rutiles from all samples of the Dronero-Sampeyre unit yield comparable results within uncertainty, at 465 ± 22°C (507 ± 21°C, n = 57) for DM19b-12a, 438 ± 25°C (482 ± 24°C, n = 29) for DM19-14a, 431 ± 26°C (475 ± 25°C, n = 51) for DM19b-14, 433 ± 13°C (477 ± 12°C, n = 60) for DM19-15a, and 426 ± 44°C (470 ± 42°C, n = 39) for the only garnet-chloritoid-bearing micaschist (DM19b-01).

Cima di Crosa unit

Sample DM19b-43 yields an average temperature of 403 ± 25°C (446 ± 24°C, n = 88).

5.2. U-Pb geochronology

A total of 25 samples were analyzed for rutile U-Pb geochronology. Among those, only 17 showed sufficiently radiogenic Pb to extract geochronological information. Four of them yielded pre-Alpine dates (Supporting Figure S3). Thirteen Alpine-related dates are presented below (Fig. 6 for rutile, Fig. 7 for titanite), and synthesized on Fig. 8. All uncertainties below are given as 2σ.

Sanfront-Pinerolo unit

Rutile in garnet-chloritoid micaschist DM19-12 yielded an isochron date of 32.7 ± 2.2 Ma (Fig. 6A).

San Chiaffredo unit

Rutile inclusions in garnet in sample DM19b-05 yielded an isochron date of 35 ± 3.5 Ma (Fig. 6B), whereas the matrix rutiles define a 33.3 ± 4.5 Ma isochron (Fig. 6C).

Brossasco-Isasca unit

Rutiles from three samples in the Brossasco-Isasca unit all yielded errorchrons. Rutile from mafic eclogite sample DM18-21 (average grain size of 168 μm) yielded an errorchron at 31.6 Ma (Fig. 6D). Rutile from pyrope whiteschist sample DM19-06 yielded an isochron at 39.7 ± 2.6 Ma for all analyses large matrix crystal (420 μm grain). Analyses located near the rim and fractures are however strongly enriched in Pb compared to the core, excluding these analyses (above 800 ppm of Pb) yielded an isochron at 37.4 ± 3.3 Ma. Smaller rutile (average grain size of 110 μm) included in garnet in the same sample yielded an errorchron of 33.1 Ma for smaller inclusions in garnet (Fig. 6E). Rutile inclusions in garnet from another pyrope whiteschist (DM19-09) yielded an errorchron at 34.0 Ma for (average grain size of 262 μm; Fig. 6F).

Rocca Solei unit

Rutiles from two micaschist samples of the Rocca Solei unit were dated in micaschists. Rutiles from sample DM19-22 yielded an isochron date of 35.9 ± 3.1 Ma (Fig. 6G), while sample DM19b-42 yielded a date of 36.3 ± 3.3 (Fig. 6H).
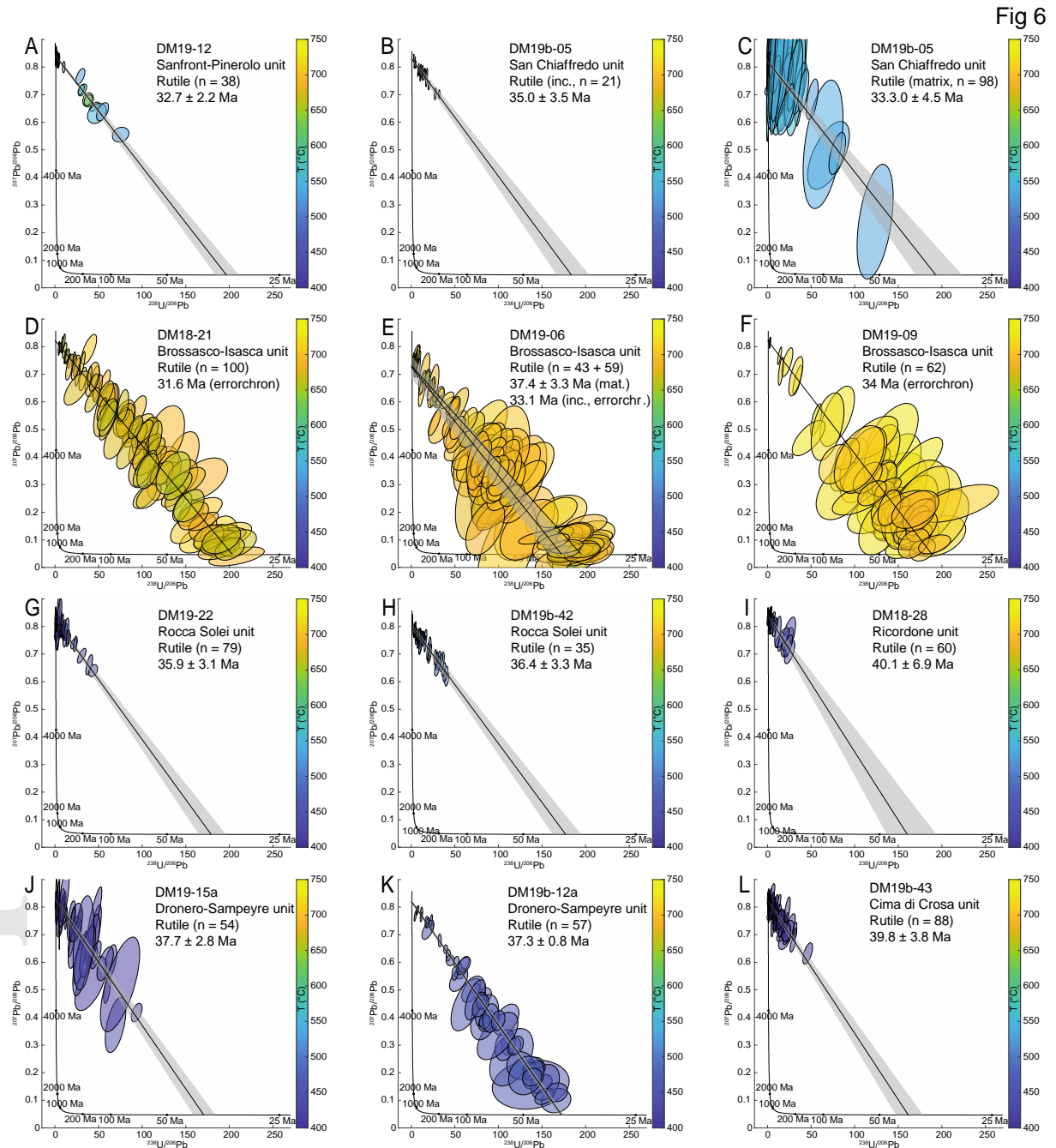

Fig. 6: Tera-Wasserburg plots and isochrons/errorchrons for Alpine peak metamorphism (rutile) in the Sanfront-Pinerolo unit (A), San Chiaffredo unit (B-C), Brossasco-Isasca unit (D-F), Rocca Solei unit (G-H), Ricordone unit (I), Dronero-Sampeyre unit (J-K) and Cima di Crosa unit (L).

Ricordone unit

The only sample in the Ricordone unit to yield an isochron is garnet-chloritoid micaschist DM18-28, dated at 40.1 ± 6.9 Ma (Fig. 6I).

Dronero-Sampeyre unit

Two samples yielded isochron dates in the Dronero-Sampeyre unit. Peak metamorphic assemblages yielded isochron dates of 37.7 ± 2.8 Ma and 37.3 ± 0.8 Ma for samples DM19-15a and DM19b-12a, respectively (Fig. 6J, K).

Cima di Crosa unit

Rutile in garnet micaschist sample DM19b-43 from the Cima di Crosa unit yielded an isochron at 39.8 ± 3.8 Ma (Fig. 6L). As in all previous samples, rutile was part of the peak metamorphic assemblage.

Retrogression in the Rocca Solei unit

Retrograde titanite after rutile in an impure marble from the Rocca Solei unit (DM19-33b) yielded a 31.2 Ma errorchron (Fig. 7).

Pre-Alpine dates

Pre-Alpine dates (Supporting Figure S3) were extracted from the Sanfront-Pinerolo unit (titanite in sample 98DM64, 291 Ma errorchron), the Rocca Solei unit (titanite in sample DM19-34c, 238 ± 32.2 Ma isochron), and Ricordone unit (two generations of rutile in sample DM19-31a with 323 and 293 Ma errorchrons and rutile in sample DM19-30, 356 ± 35.4 Ma isochron).
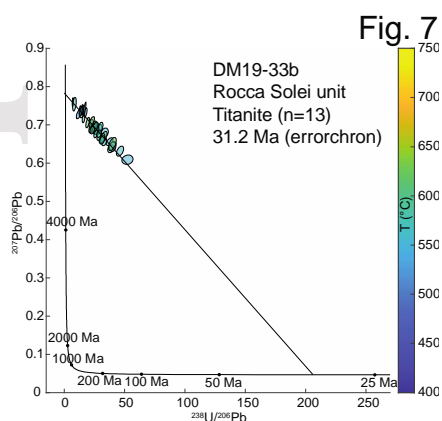

Fig. 7: Tera-Wasserburg plot and errorchron for alpine retrogression (titanite) in the Rocca Solei unit.
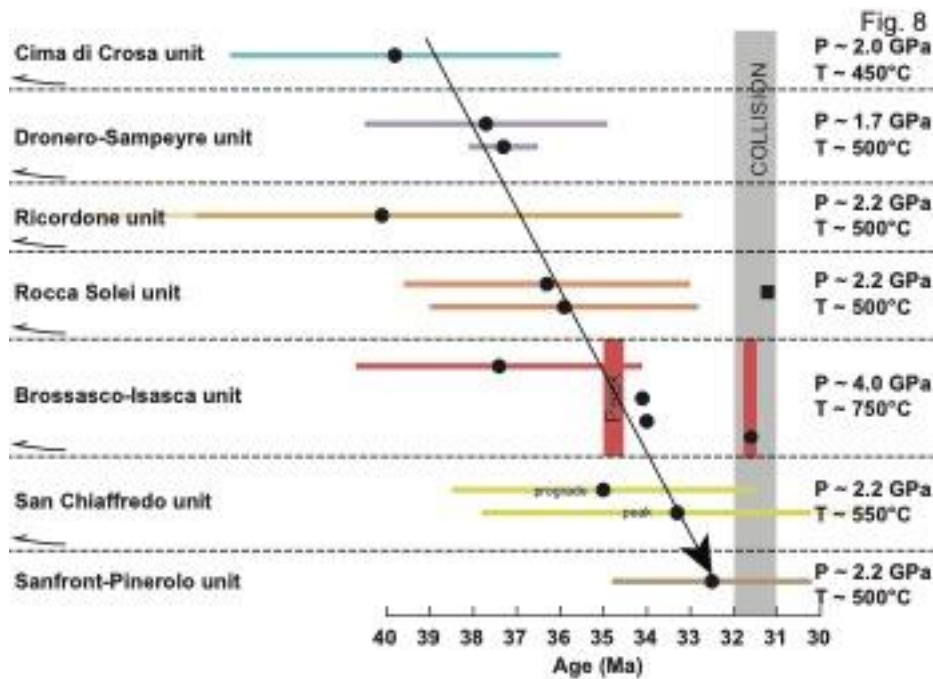
Fig. 8: Synthesis of rutile U-Pb geochronological results (circles) showing peak metamorphic ages younging downwards from the Cima di Crosa unit (~40 Ma) to the Sanfront-Pinerolo unit (~32 Ma). Peak of the UHP unit is from the literature, collision is dated with retrograde titanite (square) from this study and Rubatto and Hermann (2001) at ~32-31 Ma.

6. Discussion

6.1. Interpretation of the results and potential limitations

Temperature estimates

All units investigated in this study bear high-pressure assemblages, with garnet and chloritoid in textural equilibrium in non-UHP metapelites. Zr-in-rutile thermometry is an independent way to confirm peak temperatures calculated with thermodynamic datasets. While rutile usually forms at high grade during prograde metamorphism (i.e., close to peak), the Zr concentration of rutile may equilibrate when temperature increases (e.g., Kohn, 2020).

Peak temperatures obtained in this study are overall within 50°C of previously published estimates (Chopin et al., 1991; Henry et al., 1993; Groppo et al., 2019): the Cima di Crosa unit around 450°C (expected ~500°C), the Rocca Solei and Dronero-Sampeyre units around 450°C, the San Chiaffredo units around 500-550°C, and the Brossasco-Isasca unit at 700-750°C. Temperature estimates are slightly lower than thermodynamic predictions from the literature at low temperature, which might be due to (1) rutile growth during prograde metamorphism and limited reequilibration at higher temperature, (2) partial reequilibration during retrograde metamorphism, or (3) inaccuracy of the Kohn (2020) calibration that can yield results as much as ~40°C lower than the previous calibration (Tomkins et al., 2007), in particular at T < 700°C. Focusing on the hottest sample in each unit in fact

reduces the disagreement between rutile temperatures and literature values, and the least-retrogressed samples (garnet-bearing) always record the highest temperatures, which is compatible with fluid-assisted Zr diffusion during retrogression. Isotopic values do not seem to be affected by this phenomenon.

Sample DM19-12 from the Sanfront-Pinerolo unit shows a large scatter of Zr-in-rutile temperatures, below and above the expected temperature of ~500°C. While scatter in temperature values is common in rutile (e.g., Campomenosi et al., 2021), the scatter in this sample might be explained by the mixing of relict and newly-formed grains (although there is no sign of this in the isochron), non-reequilibrated prograde grains, or local deviations of the activities of $ZrSiO_4$ and SiO_2.

Pressure estimates of the literature: no significant deviations from lithostatic

Overpressures (i.e., deviations from lithostatic pressure) are occasionally proposed on theoretical grounds to explain metamorphic pressures and exhumation rates (e.g., for the Brossasco-Isasca unit, Ford et al., 2006; Schenker et al., 2015). However, the independent determination of peak temperatures correlated with pressure estimates, of ~750°C (see also Campomenosi et al., 2021) for the Brossasco-Isasca unit and 400-550°C for lower-pressure units argues in favor of an alignment of all units of the western Alps along a 6-8°C/km metamorphic gradient (Fig. 3) with minor deviations (Groppo et al., 2019 for Dora-Maira; Jolivet et al., 2003 and Agard, 2021 for the Western Alps). This range of gradients is compatible with slab surface temperatures under a cold subduction regime (Gerya et al., 2002; Syracuse and Van Keken, 2010; Agard et al., 2018). This alignment makes the possibility of regional overpressures improbable, because temperatures should be relatively independent of (over)pressures in this case (e.g., Schmalholz et al., 2014, their figure 13). Additionally, the homogeneity of P-T conditions for samples collected in various places and all common lithologies of the UHP unit precludes significant local overpressures in the UHP unit (unlike proposed by Luisier et al., 2019 in HP units of the Monte Rosa massif). Campomenosi et al. (2021) tried to directly measure the stress state at the time of entrapment of zircon inclusions within pyrope from the UHP whiteschists. In spite of post-entrapment plastic deformation of the garnet that contributes to reducing the apparent entrapment pressures, they showed that the deviatoric stress was likely small at the time of garnet growth. These diverse considerations justify the interpretation of metamorphic pressures as lithostatic pressures in this study, in which 4 GPa corresponds to a burial of ~120 km, assuming average upper-plate densities of 3.3-3.4 (mantle values).

Rutile U-Pb geochronology records closure in the UHP unit, crystallization in other units

To understand the rates of Pb diffusion in rutile and the significance of the dates, closure temperature was calculated with the iterative equation of Dodson (1973) for spherical crystals. Lead

diffusion coefficients were determined experimentally by Mezger et al. (1989), but were significantly revised by Cherniak (2000). The latter results are in line with analytical estimates of closure temperatures by Vry et al. (2006) and Kooijman et al. (2010). Experimental parameters for Pb diffusion should in any case be interpreted with care because experiments reached high Pb concentrations of ~4000 ppm at temperatures of 700-1100°C. This might lead to overestimation of Pb diffusivity for lower Pb contents, and hence underestimation of closure temperatures.

In order to appreciate Pb diffusion in rutile, peak temperatures and approximate cooling rates derived from the literature were used for each unit (~750°C and ~100°C.Ma^{-1} for the UHP unit and ~550°C and ~10°C.Ma^{-1} for the other units) to obtain the minimum crystal size that would be unaffected by closure of the system. According to this simulation, crystals smaller than 200 μm cannot record peak metamorphic ages in the UHP unit, whereas crystals as small as 15 μm can record peak metamorphic ages in all other units (Supporting Figure S4). This means in theory that rutile U-Pb geochronology is likely to yield cooling temperatures in the UHP unit (except for the largest crystals), and crystallization temperatures in other units, because most of the crystals analyzed were larger than 50 μm (laser spot size is 35 μm for all samples). The calculation of errorchrons for all samples of the UHP unit underlines deviations from theoretical isochrons (due to diffusion, or common-Pb inhomogeneities). It is nevertheless remarkable that rutile errorchron dates in the pyrope whiteschists of the UHP unit are correlated with the average rutile grain size and average distance to crystal rim. The largest rutile grain in pyrope whiteschists (average size of 420 μm, average distance from analysis spot to rim of rutile of ~85 μm) yields an age (at 37.4 ± 3.3 Ma) comparable within error to the peak age from the literature (around 35 Ma), while smaller rutile grains (average grain size of 260 μm, average distance to rim of 63 μm) yield dates of ~34 Ma and even smaller rutile grains (average size of 110 μm, average distance to rim of 30 μm) yield a date of ~33.1 Ma. This is in agreement with closure sizes exposed above, and compatible with diffusion over a few micrometers. This also outlines the role of garnet to shield Pb diffusion from rutile: small rutile crystals in the matrix of an UHP eclogite yield a date of 31.6 Ma (average size of ~170 μm, average distance to rim of ~35 μm).

Lead concentrations obtained on ICP-MS spots were plotted against distance from the rim across a single large rutile grain from a whiteschist of the UHP unit. Lead enrichment near the rim suggests that there might be some inward Pb diffusion in the first ~40 μm (high Pb analyses were hence discarded from the calculation), but the measurements are limited by laser spot size, potential 3D effects and entrapment of common Pb along grain boundaries (Supporting Figure S5). Attempts have been made to directly measure Pb concentration profiles with an electron probe microanalyzer, but low Pb concentrations and interference of Pb and Nb Mα rays in wavelength dispersive spectrometry prevents any measurement, even at high counting times.

No such problems were encountered for rutile in low-temperature eclogites, which yielded isochrons and dates independent of grain size, and were thus interpreted as crystallization ages. The imperfect preservation of Variscan ages in rutile (with high uncertainty, and errorchrons rather than isochrons) in our dataset also suggests incomplete resetting of the U-Pb isotopic system during Alpine metamorphism.

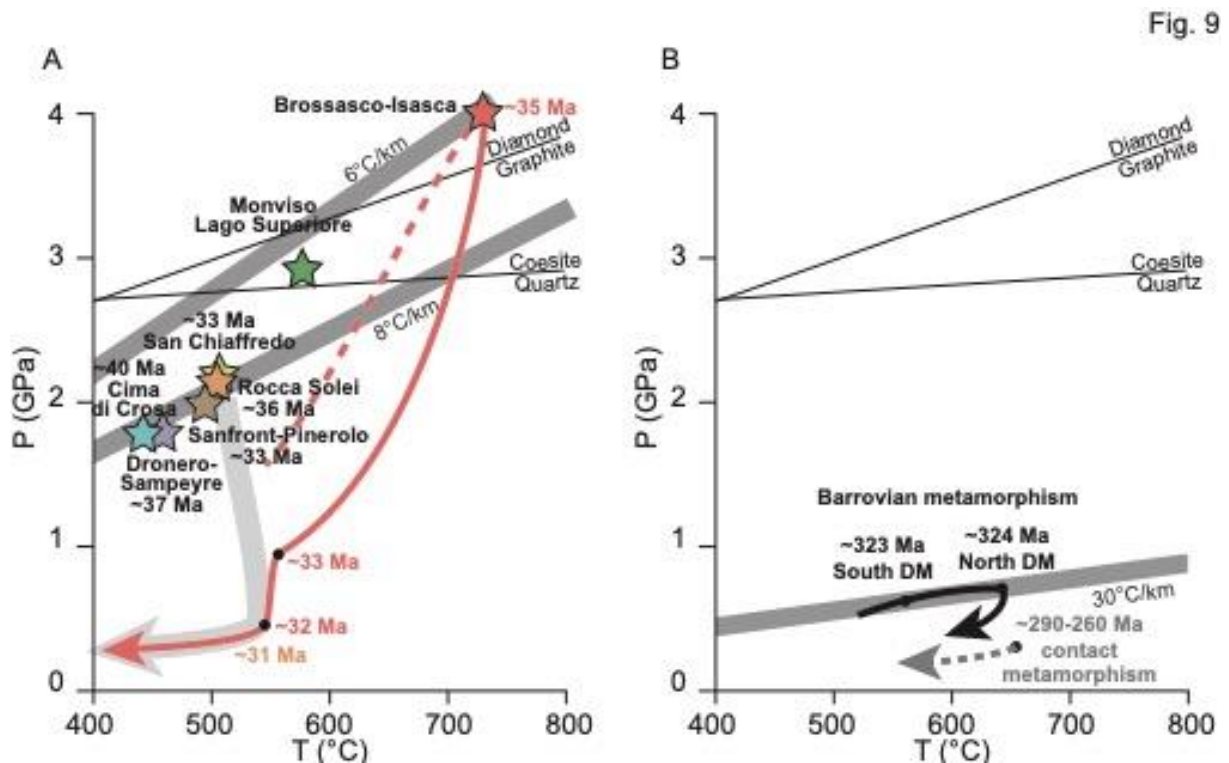## 6.2. Subduction and fast exhumation of continental slices of the Dora-Maira massif

Fig. 9: Synthesis of P-T-t paths of the main Dora-Maira units deduced from results of this study. A) Alpine evolution (additional references in Fig. 3). B) Pre-Alpine evolution (from this study for the southern Dora-Maira massif and Nosenzo et al., 2022 for the northern Dora-Maira massif).

Peak metamorphic ages in the southern Dora-Maira massif range between 40 and 32 Ma, depending on the unit considered (Fig. 8 and Fig. 9A). These results are the first reliable dates of peak metamorphism of non-UHP units, and are compatible with estimates of peak metamorphism of the Brossasco-Isasca UHP unit at 35-34 Ma. Our results show a consistent trend in the peak metamorphic ages (Fig. 8), with younger ages at the bottom of the pile, and reveal diachronous subduction of units in the southern Dora-Maira massif. All Dora-Maira units share a common shallow-depth retrogression history, marked by the dominant greenschist-facies ductile fabric observed in the massif (Chopin et al., 1991; Henry et al., 1993; Michard et al., 1995). The ~31 Ma greenschist-facies titanite age in the Rocca Solei unit allows us to date this fabric, and is more precisely constrained at

31.8 ± 0.5 Ma at midcrustal depths of 15-20 km in the Brossasco-Isasca unit (Rubatto and Hermann, 2001).

The exhumation of high-pressure rocks depends on their slicing from the downgoing plate and exhumation mechanisms (Agard et al., 2018). Peak metamorphic ages may be interpreted as ages of slicing off the downgoing plate (e.g., Bonnet et al., 2018). After peak, units are exhumed and underplated at shallower depth. The correlation found in this study between the timing of peak metamorphism and position in the nappe stack implies that (1) units were underplated sequentially beneath previously exhumed units and (2) the order of underplating is the same as that of slicing. Precise exhumation paths are only constrained in the Brossasco-Isasca unit (Rubatto and Hermann, 2001), with exhumation rates as high as 34 mm/yr during early exhumation, and progressively slowing to 16 mm/yr until the unit reached ~15 km depth. All units must have been exhumed to midcrustal (greenschist-facies) depths at 31.8 Ma. Therefore, the slowest possible exhumation rate (6.6 ± 1.6 mm/yr) is obtained for the Dronero-Sampeyre unit (the earliest unit to reach peak conditions [disregarding the Cima di Crosa unit, for which precise P-T conditions are not available]). Units below the Dronero-Sampeyre unit likely had faster average exhumation rates, of the order of ~10 mm/yr. This shows that exhumation of subducted continental crust was a continuous process that occurred at plate-tectonic rates. It may have been facilitated by a low-viscosity and dense mantle shear zone (Schmalholz and Schenker, 2016), as suggested by surface-wave tomography suggestive of a serpentinized plate interface (Zhao et al., 2020).

The greenschist-facies fabric and metamorphic event mark the last exhumation movements along the plate interface. Zircon fission tracks record fast cooling of the massif below 240 ± 20°C as early as 29.9 ± 2.8 Ma (Gebauer et al., 1997). Later cooling/exhumation was recorded by pseudotachylites formed at depths shallower than 3 km at 20.1 ± 0.5 Ma (Cosca et al., 2005; Zechmeister et al., 2007), and by apatite fission-track ages (27-13 Ma, Tricart et al., 2007; Beucher et al., 2012). This implies much slower exhumation processes (~0.3 mm/yr for the last 30 Myr, ~0.1 mm/yr for the last 20 Myr), controlled by erosion rates in the Western Alpine belt (e.g., Kuhlemann et al., 2001; Malusà et al., 2005).

A few studies have assumed that oceanic lithosphere might be exhumed along with continental crust (e.g., Lapen et al., 2007; Angiboust et al., 2011), yet our results are in accord with the results of Angiboust and Glodny (2020) showing that the Monviso ophiolite had already been exhumed to subcrustal depth at 38-36 Ma, before the exhumation of the uppermost units of the Dora-Maira nappe-stack.

6.3. Reconstitution of the European margin exposed in Dora-Maira

Nature of the Dora-Maira crust: thin portions of the upper continental crust

The Dora-Maira massif is composed of multiple nappes of continental affinity, locally intercalated with shear zones including oceanic material (e.g., the "Ophiolitiferous Band", or Valmala tectonic unit, in Henry et al., 1993 and Balestro et al., 2020, respectively). The basement of the Dora-Maira nappes is mainly Variscan upper continental crust (e.g., Nosenzo et al., 2022). The absence of lower continental crust is generally explained by asymmetric rifting of the margin (Lemoine et al., 1987), with lower crustal portions being located on the eastern margin, in the Ivrea zone (Lemoine et al., 1987). This is further confirmed by the Mg metasomatism that produced the whiteschist protolith from metagranite (Compagnoni and Hirajima, 2001), which was assigned to ultramafic-derived fluids (from talc and antigorite breakdown) during subduction (Sharp et al., 1993; Ferrando et al., 2009; Chen et al., 2016, 2019; Tian et al., 2019), implying a close spatial association of the upper continental crust with the underlying mantle.

The continental crust of Dora-Maira mainly reflects magmatic events of mostly Permian age (~304-253 Ma: Tilton et al., 1989; Bussy and Cadoppi, 1996; Gebauer et al., 1997; Paquette et al., 1999; Rubatto and Hermann, 2001), as well as regional, Barrovian metamorphism dated as Carboniferous (Nosenzo et al., 2022) and contact metamorphism associated to granitic intrusions, dated on this basis as Permian. In this study, new occurrences of pre-Alpine rutile and titanite of Carboniferous (356 ± 35 Ma, ~323 Ma) and Permian age (~292 Ma, ~291 Ma, 238 ± 32 Ma) were found in Alpine metamorphic rocks (Supporting Figure S3). Assuming a gradient of 30°C/km, relevant for Barrovian-type Carboniferous metamorphism (e.g., Faure et al., 2009; Nosenzo et al., 2022), P-T conditions of 500-560°C and 0.6 GPa are deduced from the Zr thermometry data obtained for the Carboniferous relics. These results may be compared to the Barrovian metamorphic conditions (~650°C, 0.6-0.7 GPa) preserved in garnet-staurolite micaschists of the northern Dora-Maira massif, dated at 324 ± 6 Ma (Nosenzo et al., 2022). In contrast, the Permian event is a high-temperature, low-pressure contact metamorphism as shown by the occurrence of pseudomorphs after andalusite around Permian intrusions in the (Sanfront-)Pinerolo unit (Franchi and Novarese, 1895; Bussy and Cadoppi, 1996), and after cordierite, andalusite, sillimanite and spinel around the Permian Brossasco granite (Compagnoni and Rolfo, 2003; Groppo et al., 2007a). Assuming pressures of 0.3 GPa, Zr thermometry in Permian rutile and titanite yields temperatures of ~660°C (Sanfront-Pinerolo unit), ~640°C (Rocca Solei unit) and 510°C (Ricordone unit) – whose variations might be a function of the distance to intrusion(s). These results are synthetized on Table 2 and Fig. 9B.

A consequence is that the continental crust exposed in Dora-Maira likely consists of relatively shallow portions of the Variscan orogen (there is no evidence of metamorphism deeper than 20 km, Ballèvre et al., 2020; Nosenzo et al., 2022), thinned and stretched by Permian post-collisional collapse and Jurassic rifting. The occurrence of mantle rocks, mafic magmatic rocks and overlying sediments

within the stack (the Ophiolitiferous Band) suggests that stretching was locally intense enough to exhume subcontinental mantle and generate limited amounts of magmatism.

Restoration of Dora-Maira prior to subduction: hyperextended European margin

Using the peak metamorphic ages determined in this study and the P-T-t evolution of other subducted units along the same transect, it is possible to restore the original configuration of the European margin. Parameters to consider include the convergence rates, dip of the subduction zone, depth and age of maximum burial of each unit.
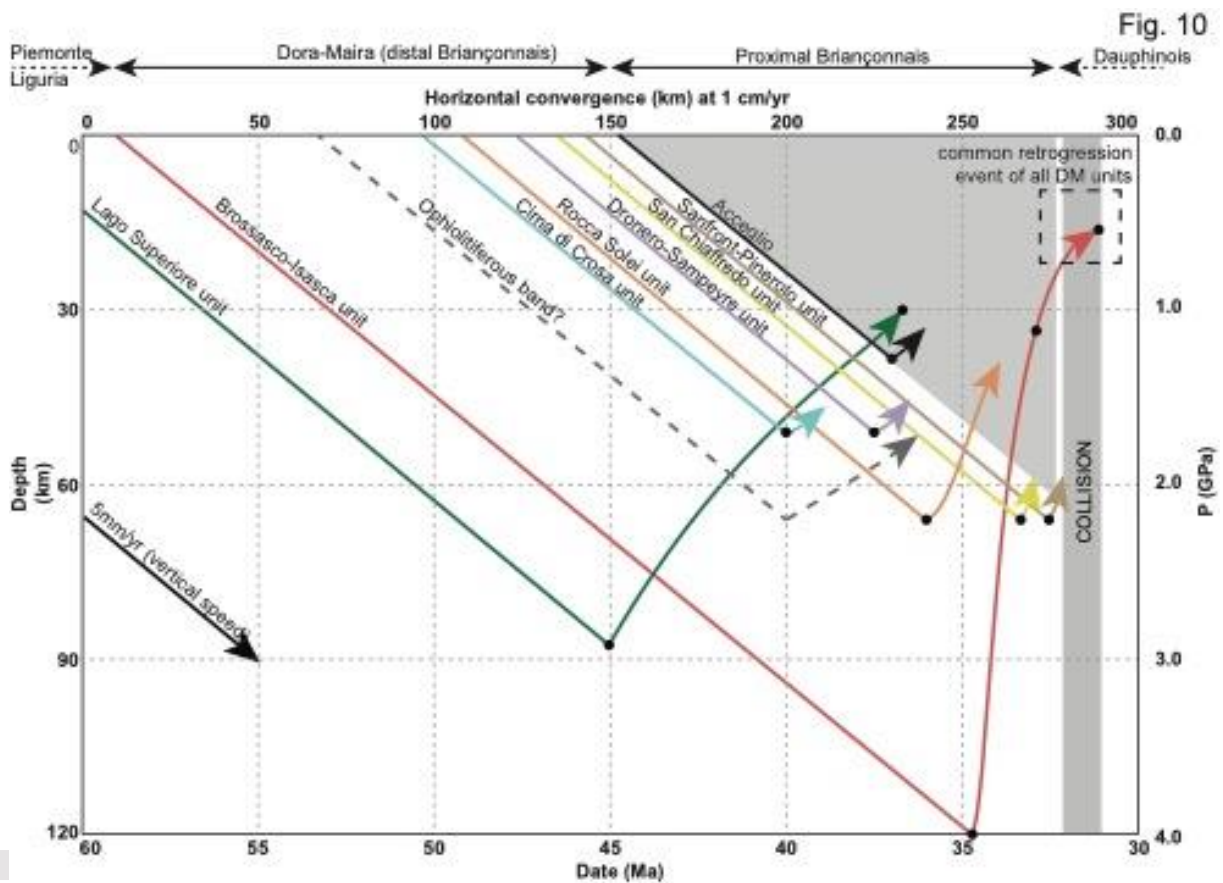

Fig. 10: Pressure (depth, temperature) – time paths for subducted units of the Piemonte-Liguria and Briançonnais domains. Subduction prograde path drawn assuming a constant vertical velocity of 5 mm/yr. Theorical horizontal convergence and vertical speed are expressed assuming a constant 1 cm/yr convergence speed, compatible with a ~30° subduction dip. Read text for details.

The direction of convergence between Adria and Europe has been estimated to have been roughly west-northwest from 70 Ma to the present on the basis of kinematic indicators from Alpine tectonites (Choukroune et al., 1986; Platt et al., 1989), and plate reconstructions (Handy et al., 2010). These plate reconstructions suggest shortening rates of 9-15 mm/yr from 70 to 20 Ma (Handy et al., 2010). Based on unfolding of cross-sections through the Swiss-Italian Alps, Schmid et al. (1996)

proposed a 5-15 mm/yr normal convergence rate from 65 to 32 Ma. Based on combined garnet Lu-Hf and Sm-Nd geochronology in UHP eclogites from Lago di Cignana, Lapen et al. (2003) proposed burial rates of Lago di Cignana rocks (Zermatt-Saas) of 2.3-4.7 mm/yr between 50 and 40 Ma, which they inferred to correspond to Europe-Adria convergence rates of 4-14 mm/yr. Similar burial values of ~4.7 mm/yr were obtained by Dragovic et al. (2020) using zoned garnet Sm-Nd geochronology, in the southern part of the Zermatt-Saas unit. In the following, a constant normal convergence rate of 10 ± 5 mm/yr between Europe and Adria at the latitude of Monviso–Dora-Maira is assumed.

Dips of the Alpine subduction zone have been proposed by several studies. Geodynamic/geometric models of the Alps generally assume dips of 20-30° (Escher and Beaumont, 1997; Pfiffner et al., 2000), comparable to slab dips in active subduction zones (e.g., Lallemand et al., 2005). Using geochronological results and convergence assumptions, Dragovic et al. (2020) obtained paleodips of 15-20° between 50 and 40 Ma at a latitude intermediate between Monte Rosa and Gran Paradiso. The current dip of the Briançonnais below Adria can be estimated from tomographic sections showing the current European root dipping between 25 and 45° below Italy (Lippitsch et al., 2003; Zhao et al., 2015; Kästle et al., 2018). Based on reconstitutions of the length of subducted units, Carry et al. (2011) proposed that paleodips reached a maximum of 60° at the latitude of Dora-Maira, but this reconstitution does not account for the shortening linked to the stack of multiple slices in Dora-Maira. In the following, a subduction dip of 30 ± 15° is assumed.

Using these parameters, we can reconstitute the pressure/temperature/depth-time of each unit, assuming lithostatic pressure and an upper-plate density of 3.4 (Fig. 10). The first unit of Dora-Maira to enter subduction was likely the Brossasco-Isasca unit (reaching a peak burial depth of 120 ± 10 km at 35 ± 1 Ma), whereas the last was the Sanfront-Pinerolo unit (reaching a peak burial depth of 66 ± 10 km at 32.7 ± 2.2 Ma). Using all these estimates and propagating uncertainty, we can reconstruct a continental margin stretched over 130 ± 60 km from the most proximal (Sanfront-Pinerolo) to the most distal (Brossasco-Isasca) portions of Dora-Maira (Fig. 11). A comparable order of magnitude is obtained by adding the exposed E-W length of all Dora-Maira slivers (although the greenschist-facies retrogression was accompanied by intense flattening and stretching and a significant portion does not crop out). West of the Schistes Lustrés and in the Acceglio half-window at the same latitude, the "proximal" Briançonnais crops out along a restored section of ~80 km (e.g., Michard and Henry, 1988; Michard et al., 2004; Ballèvre et al., 2020). Conservative estimates of the width of the Briançonnais s.l., including its distal margin (i.e., Dora-Maira) sum up to 210 ± 60 km, comparable to the ~200 km and ~240 km restored sections proposed by Ballèvre et al. (2020) and Pantet et al. (2020), respectively. This structure is mainly inherited from the Early Jurassic rifting, which has impacts far into the Dauphinois domain (e.g., in Oisans, Bellahsen et al., 2012).

In fact, the Brossasco-Isasca unit entered subduction before (~9 Myr) the other Dora-Maira units, from which it might have been separated by a largely non-recovered portion of lithosphere. The preservation of eclogite-facies assemblages in the Ophiolitiferous band (Balestro et al., 2020) and its intercalation within the Dora-Maira massif (Fig. 10) might suggest that the Brossasco-Isasca massif was once an extensional allochthon.
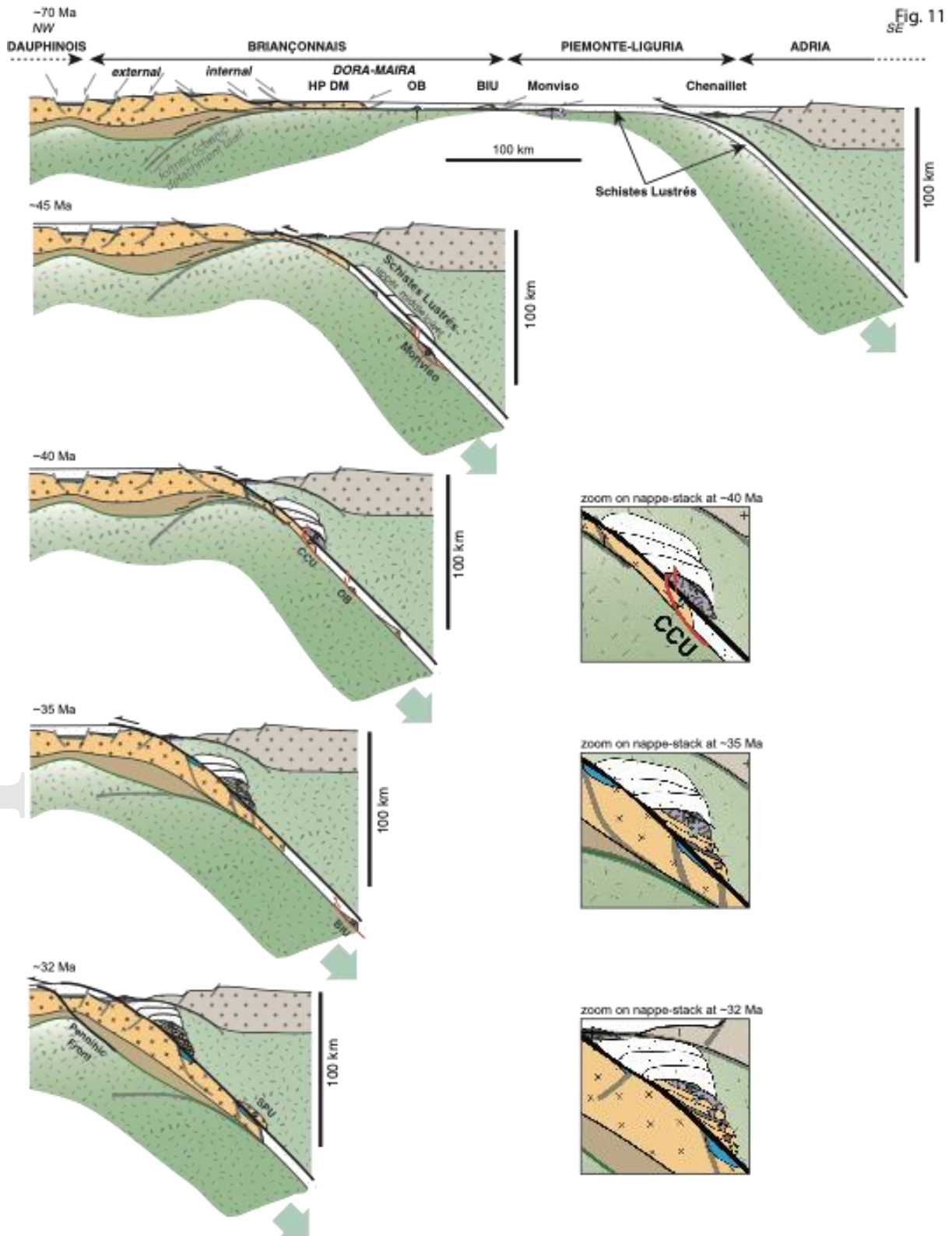
Fig. 11: Idealized evolutive reconstitution of the subduction of the European continental margin during Eocene-Oligocene, as supported by data from this study. HP DM, high-pressure units of Dora-Maira; CCU, Cima di Crosa unit; OB, Ophiolitiferous band; BIU, Brossasco-Isasca unit; SPU, Sanfront-Pinerolo unit. Modified after Agard (2021), and inspired by many authors (e.g., Ballèvre et al., 2020). Stars are located in units after reaching peaks, colors correspond to those of Fig. 2. The structure of the upper plate has been greatly simplified and tectonic slices are drawn thicker than reality for clarity. Zoomed-in squares are approximately 50 x 50 km.

While the extension of rifting structures across hundreds of kilometers is not uncommon (e.g., West European rift, Ziegler, 1992), the occurrence of thinned margin (ocean-continent transition) and extensional allochthons over distances close to a hundred kilometers are symptomatic of hyperextended margins, as is observed in today's Northern Atlantic margins (e.g., Iberia, Manatschal et al., 2001). The hyperextended nature of the European margin in the Alpine realm was revealed independently by previous studies (Manatschal, 2004; Beltrando et al., 2010; Mohn et al., 2014; Beltrando et al., 2014; Ballèvre et al., 2020), but we have here a first estimate of the geographical spread of this margin. Allochthons may in fact extend far into the Piemonte-Liguria Domain (Etirol-Levaz slice located on top of the Zermatt-Saas complex, Beltrando et al., 2010).

6.4. Integration in western Alpine tectonics

What is recovered from subduction? Evaluation across a W-E transect

Several other units metamorphosed at HP-LT conditions crop out in the continuity of the E-W transect studied here, in particular mafic-ultramafic-dominated (Monviso complex) and metasediment-dominated (Schistes Lustrés) units of the Piemonte-Liguria domain, and portions of the Briançonnais domain west of the Schistes Lustrés (Agard, 2021). The Monviso complex is interpreted to be a former oceanic core complex in a slow-spreading ocean (Lagabrielle and Cannat, 1990; Festa et al., 2015). Its main unit (Lago Superiore unit), just above the Dora-Maira complex, was metamorphosed at 2.7 GPa and 580°C (Groppo and Castelli, 2010; Angiboust et al., 2011, 2012; Locatelli et al., 2019); it reached its peak between 53 and 45 Ma (Monié and Philippot, 1989; Duchêne et al., 1997; Garber et al., 2020; Rubatto and Hermann, 2003; Rubatto and Angiboust, 2015) and was retrogressed at lower crustal depths at 42-36 Ma (Cliff et al., 1998; Angiboust and Glodny, 2020). The timing of peak metamorphism of the overlying Monviso unit, metamorphosed at 2.2 GPa and 490°C (Schwartz et al., 2000a; Angiboust et al., 2012) is unknown, but retrogression occurred at the same time as in the Lago Superiore unit (Angiboust and Glodny, 2020).

Above Monviso, the Schistes Lustrés are interpreted as an oceanic sedimentary sequence, with small ophiolitic bodies that are interpreted as oceanic core complexes (e.g., Lagabrielle et al., 2015).

The Schistes Lustrés are divided in three main bodies (e.g., Plunder et al., 2012; Herviou et al., 2022) with increasing P-T conditions from west to east, from 1.2 GPa and 300°C to 2.3 GPa and 480°C (Agard et al., 2001; Plunder et al., 2012), with the western exposures lying structurally above the eastern ones. The peak metamorphism of these units is thought to have occurred around 62-55 Ma, followed by progressive retrogression from 51 to 35 Ma (Agard et al., 2002; Villa et al., 2004).

Finally, still farther west, more-proximal portions of the European passive margin crop out below (and west of) the Schistes Lustrés: the Acceglio half-window (internal Briançonnais) and the proximal Briançonnais exposed in the Guil and Ubaye valley. Peak metamorphism in the Acceglio half-window is estimated at >1.3 GPa and 450°C (Schwartz et al., 2000b) and dated at ~37 Ma (Monié, 1990), whereas proximal Briançonnais exposures were metamorphosed at 0.6-0.8 GPa and 270-300°C (Michard et al., 2004; Lanari et al., 2012; Lanari et al., 2014; Ballèvre et al., 2020). Precise dates of peak metamorphism are not available for the low-grade exposures, but they must be younger than the youngest sediments (*Flysch Noir)* of Eocene age (Bartonian-Priabonian, i.e., 41-34 Ma; Kerckhove et al., 2005).

This allows to restore the chronology of subduction of the European lithosphere: first, ocean-derived units (sedimentary-, then mainly mafic-ultramafic-dominated rocks), then continent-derived units (distal then proximal margin). The recovery of all these units from deep subduction may have been favored by the structural inheritance of detachment faults, possibly reactivated during subduction (e.g. Agard et al., 2021).

Orogen-parallel variations in the Western Alps

The Gran Paradiso and Monte Rosa massifs are lateral equivalents of the Dora-Maira massif. Geochronological data for the Monte Rosa massif indicate peak metamorphic ages ranging between 43 Ma and 32 Ma (Lapen et al., 2007; Rubatto and Gebauer, 1999; Engi et al., 2001; cf. Chopin and Monié, 1984). Whether this variability reflects the occurrence of several tectonic slices is still debated. The Gran Paradiso massif consists of two main units, the monometamorphic Money unit, overlain by the Gran Paradiso basement complex (e.g., Manzotti et al., 2015). Both of them reached peak metamorphism at 43-41 Ma and exhumation likely occurred between 39-32 Ma (constrained by phengite Rb-Sr, phengite Ar-Ar, and monazite, allanite and xenotime U-Th-Pb geochronology, Meffan-Main et al., 2004; Rosenbaum et al., 2012; Manzotti et al., 2018). However, using monazite and allanite U-Th-Pb geochronology, Gabudianu Radulescu et al. (2009) suggested ages of prograde and peak metamorphism as young as 37.4 ± 0.9 and 33.7 ± 1.6 Ma, respectively, in contrast to other studies.

In the internal Briançonnais, dates of peak (and potentially retrograde) metamorphism (Fig. 1) were obtained at 41-36 Ma at the latitude of Monte Rosa (Markley et al., 1998), 43-37 Ma at the latitude of Gran Paradiso (Freeman et al., 1997; Villa et al., 2014), and 37-32 Ma at the latitude of

northern Dora-Maira (Strzerzynski et al., 2012). This partial record points to slightly earlier subduction of the Briançonnais domain at the latitudes of Monte Rosa and Gran Paradiso than in the Dora-Maira massif, which may suggest a diachronism of continental subduction. In fact, the existence of the Austro-Alpine (Sesia-Dent Blanche) and Valaisan domains north of the present latitude of Val di Susa is coincident with the northern termination of the Dora-Maira massif. This could highlight the existence of two domains in the Piemonte-Liguria Ocean separated by a major transfer zone affecting the structure of both margins.

What triggered collision: subduction of a thicker margin or far-field geodynamics?

The transition from subduction to collision generally occurs when convergence switches from slab subduction (where most of the excess material is "lost" into the mantle, except for some slices accreted to the trench or underplated) to widespread crustal thickening (by thrusting), leading to the formation of topography and to Barrovian metamorphism. In the Western Alps, this is marked by: (1) the end of high-pressure, low-temperature metamorphism, (2) thrusting of the Briançonnais domain over the Dauphinois domain, accommodated along the Penninic Front, (3) overfeeding of the foreland basin by erosion of newly formed topography (flysch–molasse transition), (4) minimal Barrovian metamorphism and (5) a magmatic pulse in the upper plate.

The Sanfront-Pinerolo unit is the last deep slice of the European margin recovered from subduction, and was sliced off the slab at 32.7 ± 2.2 Ma (some parts of the external Briançonnais might be even younger). This timing is compatible with the tectonic activity of the Penninic front at ~34-31 Ma (Simon-Labric et al., 2009), initiation of internal deformation within the Dauphinois domain at ~33 Ma (Bellanger et al., 2015), and the early Oligocene flysch to molasse transition (Ford and Lickorish, 2004; Ford et al., 2006; Mulder et al., 2010). Contrary to Central (Lepontine) and Eastern (Tauern) Alpine exposures (Wiederkehr et al., 2008; Scharf et al., 2013), only low-grade Barrovian conditions were reached during decompression in the Western Alps. The warming of the metamorphic gradient of the Dora-Maira units during exhumation from 6-8 °C/km to ~30°C/km is potentially one of the best witnesses of incipient Barrovian metamorphism (e.g., Soret et al., 2021). A pulse of magmatism along the Insubric line, i.e. farther north, is also observed in the tonalitic Miagliano pluton and in the calc-alkaline/shoshonitic lavas of the Biella Volcanic Sequence, emplaced at 33 and 32.5 Ma, respectively (Kapferer et al., 2012; Berger et al., 2012).

The westernmost Briançonnais exposures (Zone Houillère) show a progressive increase of the metamorphic gradient with time, up to ~15°/km (Lanari et al., 2012), while warm metamorphic gradients in the Dauphinois (~25-30°/km; e.g., Boutoux et al., 2014; Bellanger et al., 2015) are characteristic of collisional gradients. In Dora-Maira, there is no significant change of the peak

metamorphic gradient across units (Fig. 3). However, retrogression in these units proceeded under warmer gradients. This implies that subduction speed did not slow down significantly before ~32 Ma, and the gradient only increased upon collision. The increase of the metamorphic gradient and incipient collision might result either from a deceleration of convergence (shown by Handy et al., 2010 and thermomechanically modeled, e.g., Burov et al., 2014; François et al., 2014) or from the underthrusting of a much thicker and radiogenic Dauphinois-domain crust jamming the subduction zone (e.g., Burov et al., 2014). The coeval end of high-pressure metamorphism in Alpine Corsica, the Betics, northeast Algeria, Calabria, and the Western Alps however suggests that collision might be a consequence of a change in regional geodynamics (with implications on convergence rates) due to slab retreat in the western Mediterranean region (Vignaroli et al., 2008; Romagny et al., 2020).

Conclusions:

This study demonstrates the utility and pitfalls of *in situ* rutile U-Pb geochronology to assess the timing and conditions of high-pressure, low-temperature metamorphism. It shows that rutile U-Pb dates can generally be interpreted as crystallization ages in subduction complexes, except for the highest-grade units. We confirm that the whole Dora-Maira transect experienced upper-blueschist- or eclogite-facies metamorphism during Alpine subduction, with P-T gaps between units. All units reached peak conditions over a time span of ~8 Myr, and each of them started to be exhumed at ~cm/yr rates directly after reaching peak conditions. This proves that exhumation of small portions of subducted continental crust is a continuous process while subduction is ongoing: the main recovery filter of high-pressure rocks is slicing from the subducting plate. We postulate that subduction of continental crust was a long-lived (~25 Myr) process in the Western Alps. It was facilitated by the limited thickness of the subducting continental crust, strongly thinned and extended during rifting: the Dora-Maira massif is reconstituted as a ~130 ± 60 km-long hyperextended margin, part of the distal Briançonnais domain (European plate) with intercalated portions of oceanic lithosphere (ocean-continent transition). This study calls for detailed estimates of variations of burial rates at different times of the continental subduction and for detailed geochronological study of the proximal Briançonnais.

Data Availability Statement:

The GPS location of samples and U-Pb-trace element data for rutile and titanite analyses are available on Zenodo via doi.org/10.5281/zenodo.6340223.

References:

Agard, P. (2021). Subduction of oceanic lithosphere in the Alps: Selective and archetypal from (slow-spreading) oceans. *Earth-Science Reviews*, 103517.

Agard, P., Jolivet, L., & Goffé, B. (2001). Tectonometamorphic evolution of the Schistes Lustrés Complex; implications for the exhumation of HP and UHP rocks in the Western Alps. *Bulletin de la Société géologique de France*, *172*(5), 617-636.

Agard, P., Monié, P., Jolivet, L., & Goffé, B. (2002). Exhumation of the Schistes Lustrés complex: in situ laser probe $^{40}Ar/^{39}Ar$ constraints and implications for the Western Alps. *Journal of metamorphic Geology*, *20*(6), 599-618.

Agard, P., Yamato, P., Jolivet, L., & Burov, E. (2009). Exhumation of oceanic blueschists and eclogites in subduction zones: timing and mechanisms. *Earth-Science Reviews*, *92*(1-2), 53-79.

Agard, P., Plunder, A., Angiboust, S., Bonnet, G., & Ruh, J. (2018). The subduction plate interface: rock record and mechanical coupling (from long to short timescales). *Lithos*, *320*, 537-566.

Agard, P., & Vitale-Brovarone, A. (2013). Thermal regime of continental subduction: the record from exhumed HP–LT terranes (New Caledonia, Oman, Corsica). *Tectonophysics*, *601*, 206-215.

Angiboust, S., Agard, P., Raimbourg, H., Yamato, P., & Huet, B. (2011). Subduction interface processes recorded by eclogite-facies shear zones (Monviso, W. Alps). *Lithos*, *127*(1-2), 222-238.

Angiboust, S., & Glodny, J. (2020). Exhumation of eclogitic ophiolitic nappes in the W. Alps: New age data and implications for crustal wedge dynamics. *Lithos*, *356*, 105374.

Angiboust, S., Langdon, R., Agard, P., Waters, D., & Chopin, C. (2012). Eclogitization of the Monviso ophiolite (W. Alps) and implications on subduction dynamics. *Journal of Metamorphic Geology*, *30*(1), 37-61.

Aleinikoff, J. N., Wintsch, R. P., Tollo, R. P., Unruh, D. M., Fanning, C. M., & Schmitz, M. D. (2007). Ages and origins of rocks of the Killingworth dome, south-central Connecticut: Implications for the tectonic evolution of southern New England. *American Journal of Science*, *307*(1), 63-118.

Arnaud, N. O., & Kelley, S. P. (1995). Evidence for excess argon during high pressure metamorphism in the Dora Maira Massif (western Alps, Italy), using an ultra-violet laser ablation microprobe ^{40}Ar-^{39}Ar technique. *Contributions to Mineralogy and Petrology*, *121*(1), 1-11.

Avigad, D., Chopin, C., & Le Bayon, R. (2003). Thrusting and extension in the southern Dora-Maira ultra-high-pressure massif (Western Alps): view from below the coesite-bearing unit. *The Journal of geology*, *111*(1), 57-70.

Balestro, G., Festa, A., & Tartarotti, P. (2015). Tectonic significance of different block-in-matrix structures in exhumed convergent plate margins: examples from oceanic and continental HP rocks in Inner Western Alps (northwest Italy). *International Geology Review*, *57*(5-8), 581-605.

Balestro, G., Fioraso, G., & Lombardo, B. (2011). Geological map of the upper Pellice Valley (Italian Western Alps). *Journal of Maps*, *7*(1), 634-654.

Balestro, G., Nosenzo, F., Cadoppi, P., Fioraso, G., Groppo, C., & Festa, A. (2020). Geology of the southern Dora-Maira Massif: insights from a sector with mixed ophiolitic and continental rocks (Valmala tectonic unit, Western Alps). *Journal of Maps*, *16*(2), 736-744.

Ballèvre, M., Camonin, A., Manzotti, P., & Poujol, M. (2020). A step towards unraveling the paleogeographic attribution of pre-Mesozoic basement complexes in the Western Alps based on U–Pb geochronology of Permian magmatism. *Swiss Journal of Geosciences*, *113*(1), 1-28.

Bellahsen, N., Jolivet, L., Lacombe, O., Bellanger, M., Boutoux, A., Garcia., S,... & Gumiaux, C. (2012). Mechanisms of margin inversion in the external Western Alps: Implications for crustal rheology. *Tectonophysics*, *560*, 62-83.

Bellanger, M., Augier, R., Bellahsen, N., Jolivet, L., Monié, P., Baudin, T., & Beyssac, O. (2015). Shortening of the European Dauphinois margin (Oisans Massif, Western Alps): New insights from RSCM maximum temperature estimates and ^{40}Ar/^{39}Ar in situ dating. *Journal of Geodynamics*, *83*, 37-64.

Beltrando, M., Manatschal, G., Mohn, G., Dal Piaz, G. V., Brovarone, A. V., & Masini, E. (2014). Recognizing remnants of magma-poor rifted margins in high-pressure orogenic belts: The Alpine case study. *Earth-Science Reviews*, *131*, 88-115.

Beltrando, M., Rubatto, D., & Manatschal, G. (2010). From passive margins to orogens: The link between ocean-continent transition zones and (ultra) high-pressure metamorphism. *Geology*, *38*(6), 559-562.

Berger, A., Thomsen, T. B., Ovtcharova, M., Kapferer, N., & Mercolli, I. (2012). Dating emplacement and evolution of the orogenic magmatism in the internal Western Alps: 1. The Miagliano Pluton. *Swiss Journal of Geosciences*, *105*(1), 49-65.

Beucher, R., van der Beek, P., Braun, J., & Batt, G. E. (2012). Exhumation and relief development in the Pelvoux and Dora-Maira massifs (western Alps) assessed by spectral analysis and inversion of thermochronological age transects. *Journal of Geophysical Research: Earth Surface*, *117*(F3).

Biino, G., & Compagnoni, R. (1992). Very-high pressure metamorphism of the Brossasco coronite metagranite, southern Dora Maira Massif, Western Alps. *Schweizerische Mineralogische und Petrographische Mitteilungen*, *72*, 347-363.

Bonnet, G., Agard, P., Angiboust, S., Monié, P., Jentzer, M., Omrani J., ... & Fournier, M. (2018). Tectonic slicing and mixing processes along the subduction interface: The Sistan example (Eastern Iran). *Lithos*, *310*, 269-287.

Bracciali, L., Parrish, R. R., Horstwood, M. S., Condon, D. J., & Najman, y. (2013). UPb LA-(MC)-ICP-MS dating of rutile: New reference materials and applications to sedimentary provenance. *Chemical Geology*, *347*, 82-101.

Bruno, M., Compagnoni, R., Hirajima, T., & Rubbo, M. (2002). Jadeite with the Ca-Eskola molecule from an ultra-high pressure metagranodiorite, Dora-Maira Massif, Western Alps. *Contributions to Mineralogy and Petrology*, *142*(5), 515-519.

Bruno, M., Compagnoni, R., & Rubbo, M. (2001). The ultra-high pressure coronitic and pseudomorphous reactions in a metagranodiorite from the Brossasco-Isasca Unit, Dora-Maira Massif, western Italian Alps: a petrographic study and equilibrium thermodynamic modelling. *Journal of Metamorphic Geology*, *19*(1), 33-43.

Burov, E., François, T., Yamato, P., & Wolf, S. (2014). Mechanisms of continental subduction and exhumation of HP and UHP rocks. *Gondwana Research*, *25*(2), 464-493.

Bussy, F., & Cadoppi, P. (1996). U-Pb zircon dating of granitoids from the Dora-Maira massif (western Italian Alps). *Schweizerische Mineralogische und Petrographische Mitteilungen*, *76*, 217-233.

Campomenosi, N., Scambelluri, M., Angel, R. J., Hermann, J., Mazzucchelli, M. L., Mihailova, B., ... & Alvaro, M. (2021). Using the elastic properties of zircon-garnet host-inclusion pairs for thermobarometry of the ultrahigh-pressure Dora-Maira whiteschists: problems and perspectives. *Contributions to Mineralogy and Petrology*, *176*(5), 1-17.

Castelli, D., Rolfo, F., Groppo, C., & Compagnoni, R. (2007). Impure marbles from the UHP Brossasco-Isasca Unit (Dora-Maira Massif, western Alps): evidence for Alpine equilibration in the diamond stability field and evaluation of the X (CO_2) fluid evolution. *Journal of Metamorphic Geology*, *25*(6), 587-603.

Carry, N., Gueydan, F., Marquer, D., & Brun, J. P. (2011). HP–UHP metamorphism as an indicator of slab dip variations in the Alpine arc. *International Journal of Earth Sciences*, *100*(5), 1087-1094.

Ceriani, S., Fügenschuh, B., & Schmid, S. M. (2001). Multi-stage thrusting at the"Peninic Front" in the Western Alps between Mont Blanc and Pelvoux massifs. *International Journal of Earth Sciences*, *90*(3), 685-702.

Chen, Y. X., Lu, W., He, Y., Schertl, H. P., Zheng, Y. F., Xiong, J. W., & Zhou, K. (2019). Tracking Fe mobility and Fe speciation in subduction zone fluids at the slab-mantle interface in a subduction channel: A tale of whiteschist from the Western Alps. *Geochimica et Cosmochimica Acta*, 267, 1-16.

Chen, Y. X., Schertl, H. P., Zheng, Y. F., Huang, F., Zhou, K., & Gong, Y. Z. (2016). Mg–O isotopes trace the origin of Mg-rich fluids in the deeply subducted continental crust of Western Alps. *Earth and Planetary Science Letters*, *456*, 157-167.

Chen, Y. X., Zhou, K., Zheng, Y. F., & Schertl, H. P. (2017). Zircon geochemical constraints on the protolith nature and metasomatic process of the Mg-rich whiteschist from the Western Alps. *Chemical Geology*, 467, 177-195.

Cherniak, D. J. (2000). Pb diffusion in rutile. *Contributions to Mineralogy and Petrology*, *139*(2), 198-207.

Chopin, C. (1984). Coesite and pure pyrope in high-grade blueschists of the Western Alps: a first record and some consequences. *Contributions to Mineralogy and Petrology*, *86*(2), 107-118.

Chopin, C. (2003). Ultrahigh-pressure metamorphism: tracing continental crust into the mantle. *Earth and Planetary Science Letters*, *212*(1-2), 1-14.

Chopin, C., Henry, C., & Michard, A. (1991). Geology and petrology of the coesite-bearing terrain, Dora Maira massif, Western Alps. *European Journal of Mineralogy*, *3*(2), 263-291.

Chopin, C., & Monié, P. (1984). A unique magnesiochloritoid-bearing, high-pressure assemblage from the Monte Rosa, Western Alps: petrologic and ^{40}Ar-^{39}Ar radiometric study. *Contributions to Mineralogy and Petrology*, *87*(4), 388-398.

Chopin, C., & Schertl, H. P. (1999). The UHP unit in the Dora-Maira massif, western Alps. *International Geology Review*, *41*(9), 765-780.

Choukroune, P., Ballèvre, M., Cobbold, P., Gautier, Y., Merle, O., & Vuichard, J. P. (1986). Deformation and motion in the western Alpine Arc. *Tectonics*, *5*(2), 215-226.

Cliff, R. A., Barnicoat, A. C., & Inger, S. (1998). Early Tertiary eclogite facies metamorphism in the Monviso Ophiolite. *Journal of Metamorphic Geology*, *16*(3), 447-455.

Compagnoni, R., Hirajima, T. and Chopin, C. (1995). Ultra-high-pressure metamorphic rocks in the western Alps. In Coleman, R.G. and Wang, X. (Ed.). *Ultrahigh Pressure Metamorphism* (206-243). Cambridge: Cambridge University Press.

Compagnoni, R., & Hirajima, T. (2001). Superzoned garnets in the coesite-bearing Brossasco-Isasca Unit, Dora-Maira massif, Western Alps, and the origin of the whiteschists. *Lithos*, *57*(4), 219-236.

Compagnoni, R., & Rolfo, F. (2003). UHPM units in the Western Alps. *Ultrahigh pressure metamorphism*, EMU Notes volume *5*, 13-49.

Compagnoni, R., Rolfo, F., Groppo, C., Hirajima, T., & Turello, R. (2012). Geological map of the ultra-high pressure Brossasco-Isasca unit (Western Alps, Italy). *Journal of Maps*, *8*(4), 465-472.

Cosca, M. A., Caby, R., & Bussy, F. (2005). Geochemistry and $^{40}Ar/^{39}Ar$ geochronology of pseudotachylyte associated with UHP whiteschists from the Dora Maira massif, Italy. *Tectonophysics*, *402*(1-4), 93-110.

Dal Piaz, G. V., & Lombardo, B. (1986). Early Alpine eclogite metamorphism in the Penninic Monte Rosa-Gran Paradiso basement nappes of the northwestern Alps. *Geol. Soc. Am. Mem*, *164*, 249-265.

Debelmas, J., & Lemoine, M. (1970). The western Alps: palaeogeography and structure. *Earth-Science Reviews*, *6*(4), 221-256.

Di Vincenzo, G., Tonarini, S., Lombardo, B., Castelli, D., & Ottolini, L. (2006). Comparison of $^{40}Ar–^{39}Ar$ and Rb–Sr data on phengites from the UHP Brossasco–Isasca Unit (Dora Maira Massif, Italy): implications for dating white mica. *Journal of Petrology*, *47*(7), 1439-1465.

Dragovic, B., Angiboust, S., & Tappa, M. J. (2020). Petrochronological close-up on the thermal structure of a paleo-subduction zone (W. Alps). *Earth and Planetary Science Letters*, *547*, 116446.

Dodson, M. H. (1973). Closure temperature in cooling geochronological and petrological systems. *Contributions to Mineralogy and Petrology*, *40*(3), 259-274.

Duchêne, S., Blichert-Toft, J., Luais, B., Télouk, P., Lardeaux, J. M., & Albarède, F. (1997). The Lu–Hf dating of garnets and the ages of the Alpine high-pressure metamorphism. *Nature*, *387*(6633), 586-589.

Engi, M., Scherrer, N., & Burri, T. (2001). Metamorphic evolution of pelitic rocks of the Monte Rosa nappe: Constraints from petrology and single grain monazite age data. *Schweizerische Mineralogische und Petrographische Mitteilungen*, *81*, 305-328.

Escher, A., & Beaumont, C. (1997). Formation, burial and exhumation of basement nappes at crustal scale: a geometric model based on the Western Swiss-Italian Alps. *Journal of structural Geology*, *19*(7), 955-974.

Ewing, T. A. (2011). Hf isotope analysis and U-Pb geochronology of rutile: technique development and application to a lower crustal section (Ivrea-Verbano Zone, Italy).

Faure, M., Lardeaux, J. M., & Ledru, P. (2009). A review of the pre-Permian geology of the Variscan French Massif Central. *Comptes rendus géoscience*, *341*(2-3), 202-213.

Ferrando, S., Frezzotti, M. L., Petrelli, M., & Compagnoni, R. (2009). Metasomatism of continental crust during subduction: the UHP whiteschists from the Southern Dora-Maira Massif (Italian Western Alps). *Journal of Metamorphic Geology*, *27*(9), 739-756.

Ferrando, S., Groppo, C., Frezzotti, M. L., Castelli, D., & Proyer, A. (2017). Dissolving dolomite in a stable UHP mineral assemblage: Evidence from Cal-Dol marbles of the Dora-Maira Massif (Italian Western Alps). *American Mineralogist*, *102*(1), 42-60.

Festa, A., Balestro, G., Dilek, Y., & Tartarotti, P. (2015). A Jurassic oceanic core complex in the high-pressure Monviso ophiolite (western Alps, NW Italy). *Lithosphere*, *7*(6), 646-652.

Ford, M., Duchêne, S., Gasquet, D., & Vanderhaeghe, O. (2006). Two-phase orogenic convergence in the external and internal SW Alps. *Journal of the Geological Society*, *163*(5), 815-826.

Ford, M., & Lickorish, W. H. (2004). Foreland basin evolution around the western Alpine Arc. *Geological Society, London, Special Publications*, *221*(1), 39-63.

Franchi, S., & Novarese, V. (1895). Appunti geologici e petrografici sui dintorni di Pinerolo. *Boll. R. Com. Geol. It.*, 26, 385-429.

François, T., Burov, E., Agard, P., & Meyer, B. (2014). Buildup of a dynamically supported orogenic plateau: Numerical modeling of the Zagros/Central Iran case study. *Geochemistry, Geophysics, Geosystems*, *15*(6), 2632-2654.

Freeman, S. R., Inger, S., Butler, R. W. H., & Cliff, R. A. (1997). Dating deformation using Rb-Sr in white mica: Greenschist facies deformation ages from the Entrelor shear zone, Italian Alps. *Tectonics*, *16*(1), 57-76.

Gabudianu Radulescu, I., Rubatto, D., Gregory, C., & Compagnoni, R. (2009). The age of HP metamorphism in the Gran Paradiso Massif, Western Alps: a petrological and geochronological study of "silvery micaschists". *Lithos*, 110(1-4), 95-108.

Ganne, J., Bertrand, J. M., Fudral, S., Marquer, D., & Vidal, O. (2007). Structural and metamorphic evolution of the Ambin massif (western Alps): toward a new alternative exhumation model for the Briançonnais domain. *Bulletin de la Société Géologique de France*, *178*(6), 437-458.

Garber, J. M., Hacker, B. R., Kylander-Clark, A. R. C., Stearns, M., & Seward, G. (2017). Controls on trace element uptake in metamorphic titanite: Implications for petrochronology. *Journal of Petrology*, *58*(6), 1031-1057.

Garber, J. M., Smye, A. J., Feineman, M. D., Kylander-Clark, A. R., & Matthews, S. (2020). Decoupling of zircon U–Pb and trace-element systematics driven by U diffusion in eclogite-facies zircon (Monviso meta-ophiolite, W. Alps). *Contributions to Mineralogy and Petrology*, *175*, 1-25.

Gauthiez-Putallaz, L., Rubatto, D., & Hermann, J. (2016). Dating prograde fluid pulses during subduction by in situ U–Pb and oxygen isotope analysis. *Contributions to Mineralogy and Petrology*, *171*(2), 15.

Gebauer, D., Schertl, H. P., Brix, M., & Schreyer, W. (1997). 35 Ma old ultrahigh-pressure metamorphism and evidence for very rapid exhumation in the Dora Maira Massif, Western Alps. *Lithos*, *41*(1-3), 5-24.

Gerya, T. V., Stöckhert, B., & Perchuk, A. L. (2002). Exhumation of high-pressure metamorphic rocks in a subduction channel: A numerical simulation. *Tectonics*, *21*(6), 6-1.

Groppo, C., & Castelli, D. (2010). Prograde P–T evolution of a lawsonite eclogite from the Monviso meta-ophiolite (Western Alps): dehydration and redox reactions during subduction of oceanic FeTi-oxide gabbro. *Journal of Petrology*, *51*(12), 2489-2514.

Groppo, C. T., Castelli, D. C. C., & Rolfo, F. (2007a). HT, Pre-Alpine relics in a spinel-bearing dolomite marble from the UHP Brossasco-Isasca Unit (Dora-Maira Massif, western Alps). *Periodico di Mineralogia*, 76, 155-168.

Groppo, C., Ferrando, S., Gilio, M., Botta, S., Nosenzo F., Balestro, G., ... & Rolfo, F. (2019). What's in the sandwich? New P–T constraints for the (U) HP nappe stack of southern Dora-Maira Massif (Western Alps). *European Journal of Mineralogy*, *31*(4), 665-683.

Groppo, C., Lombardo, B., Castelli, D., & Compagnoni, R. (2007b). Exhumation history of the UHPM Brossasco-Isasca Unit, Dora-Maira Massif, as inferred from a phengite-amphibole eclogite. *International Geology Review*, *49*(2), 142-168.

Hacker, B. R., & Gerya, T. V. (2013). Paradigms, new and old, for ultrahigh-pressure tectonism. *Tectonophysics*, *603*, 79-88.

Hacker, B. R., Ratschbacher, L., & Liou, J. G. (2004). Subduction, collision and exhumation in the ultrahigh-pressure Qinling-Dabie orogen. *Geological Society, London, Special Publications*, *226*(1), 157-175.

Handy, M. R., Schmid, S. M., Bousquet, R., Kissling, E., & Bernoulli, D. (2010). Reconciling plate-tectonic reconstructions of Alpine Tethys with the geological–geophysical record of spreading and subduction in the Alps. *Earth-Science Reviews*, *102*(3-4), 121-158.

Hayden, L. A., Watson, E. B., & Wark, D. A. (2008). A thermobarometer for sphene (titanite). *Contributions to Mineralogy and Petrology*, *155*(4), 529-'40.

Henry, C. (1990). L'unité à coesite du massif Dora-Maira dans son cadre pétrologique et structural (Alpes occidentales, Italie). *PhD thesis, Université Pierre et Marie Curie (Paris 6)*. *Mém. Sci. Terre,* n° 90-22**,** 453 p., https://hal.archives-ouvertes.fr/tel-03511047.

Henry, C., Michard, A., & Chopin, C. (1993). Geometry and structural evolution of ultra-high-pressure and high-pressure rocks from the Dora-Maira massif, Western Alps, Italy. *Journal of Structural Geology*, *15*(8), 965-981.

Hermann, J. (2003). Experimental evidence for diamond-facies metamorphism in the Dora-Maira massif. *Lithos*, *70*(3-4), 163-182.

Herviou, C., Agard, P., Plunder, A., Mendes, K., Verlaguet, A., Deldicque, D., & Cubas, N. (2022). Subducted fragments of the Liguro-Piemont ocean, Western Alps: Spatial correlations and offscraping mechanisms during subduction. *Tectonophysics*, 229267.

Jochum, K. P., Weis, U., Stoll, B., Kuzmin, D., Yang, Q., Raczek, I., ... & Enzweiler, J. (2011). Determination of reference values for NIST SRM 610–617 glasses following ISO guidelines. *Geostandards and Geoanalytical Research*, *35*(4), 397-429.

Jochum, K. P., Willbold, M., Raczek, I., Stoll, B., & Herwig, K. (2005). Chemical Characterisation of the USGS Reference Glasses GSA-1G, GSC-1G, GSD-1G, GSE-1G, BCR-2G, BHVO-2G and BIR-1G Using EPMA, ID-TIMS, ID-ICP-MS and LA-ICP-MS. *Geostandards and Geoanalytical Research, 29*(3), 285-302.

Jolivet, L., Faccenna, C., Goffé, B., Burov, E., & Agard, P. (2003). Subduction tectonics and exhumation of high-pressure metamorphic rocks in the Mediterranean orogens. *American Journal of Science*, *303*(5), 353-409.

Kästle, E. D., El-Sharkawy, A., Boschi, L., Meier, T., Rosenberg, C., Bellahsen, N., ... & Weidle, C. (2018). Surface wave tomography of the Alps using ambient-noise and earthquake phase velocity measurements. *Journal of Geophysical Research: Solid Earth*, *123*(2), 1770-1792.

Kapferer, N., Mercolli, I., Berger, A., Ovtcharova, M., & Fügenschuh, B. (2012). Dating emplacement and evolution of the orogenic magmatism in the internal Western Alps: 2. The Biella Volcanic Suite. *Swiss Journal of Geosciences*, *105*(1), 67-84.

Kerckhove, C., & Monjuvent, G. (1979). Notice explicative de la feuille Gap à 1/250.000.

Kerckhove, C., Gidon, M., Pairis, J.L. (2005). Notice explicative de la feuille Embrun-Guillestre à 1/50.000.

Kienast, J. R., Lombardo, B., Biino, C., & Pinardon, J. L. (1991). Petrology of very-high-pressure eclogitic rocks from the Brossasco-Isasca Complex, Dora-Maira Massif, Italian Western Alps. *Journal of Metamorphic Geology*, *9*(1), 19-34.

Kohn, M. J. (2020). A refined zirconium-in-rutile thermometer. *American Mineralogist*, *105*(6), 963-971.

Kooijman, E., Mezger, K., & Berndt, J. (2010). Constraints on the U–Pb systematics of metamorphic rutile from in situ LA-ICP-MS analysis. *Earth and Planetary Science Letters*, *293*(3-4), 321-330.

Kylander-Clark, A. R. C., Hacker, B. R., & Mattinson, J. M. (2008). Slow exhumation of UHP terranes: titanite and rutile ages of the Western Gneiss Region, Norway. *Earth and Planetary Science Letters*, *272*(3-4), 531-540.

Kylander-Clark, A. R., Hacker, B. R., & Mattinson, C. G. (2012). Size and exhumation rate of ultrahigh-pressure terranes linked to orogenic stage. *Earth and Planetary Science Letters*, *321*, 115-120.

Kuhlemann, J., Frisch, W., Dunkl, I., & Székely, B. (2001). Quantifying tectonic versus erosive denudation by the sediment budget: The Miocene core complexes of the Alps. *Tectonophysics*, *330*(1-2), 1-23.

Lagabrielle, Y., & Cannat, M. (1990). Alpine Jurassic ophiolites resemble the modern central Atlantic basement. *Geology*, *18*(4), 319-322.

Lagabrielle, Y., Brovarone, A. V., & Ildefonse, B. (2015). Fossil oceanic core complexes recognized in the blueschist metaophiolites of Western Alps and Corsica. *Earth-Science Reviews*, *141*, 1-26.

Lallemand, S., Heuret, A., & Boutelier, D. (2005). On the relationships between slab dip, back-arc stress, upper plate absolute motion, and crustal nature in subduction zones. *Geochemistry, Geophysics, Geosystems*, *6*(9).

Lanari, P., Guillot, S., Schwartz, S., Vidal, O., Tricart, P., Riel, N., & Beyssac, O. (2012). Diachronous evolution of the alpine continental subduction wedge: evidence from P–T estimates in the Briançonnais Zone houillère (France–Western Alps). *Journal of Geodynamics*, *56*, 39-54.

Lanari, P., Rolland, Y., Schwartz, S., Vidal, O., Guillot, S., Tricart, P., & Dumont, T. (2014). P–T–t estimation of deformation in low-grade quartz-feldspar-bearing rocks using thermodynamic modelling and $^{40}Ar/^{39}Ar$ dating techniques: example of the Plan-de-Phasy shear zone unit (Briançonnais Zone, Western Alps). *Terra Nova*, *26*(2), 130-138.

Lapen, T. J., Johnson, C. M., Baumgartner, L. P., Dal Piaz, G. V., Skora, S., & Beard, B. L. (2007). Coupling of oceanic and continental crust during Eocene eclogite-facies metamorphism: evidence from the Monte Rosa nappe, western Alps. *Contributions to Mineralogy and Petrology*, *153*(2), 139-157.

Lapen, T. J., Johnson, C. M., Baumgartner, L. P., Mahlen, N. J., Beard, B. L., & Amato, J. M. (2003). Burial rates during prograde metamorphism of an ultra-high-pressure terrane: an example from Lago di Cignana, western Alps, Italy. *Earth and Planetary Science Letters*, *215*(1-2), 57-72.

Lemoine, M., & Trümpy, R. (1987). Pre-oceanic rifting in the Alps. *Tectonophysics*, *133*(3-4), 305-320.

Lenze, A., & Stöckhert, B. (2007). Microfabrics of UHP metamorphic granites in the Dora Maira Massif, western Alps—no evidence of deformation at great depth. *Journal of Metamorphic Geology*, *25*(4), 461-475.

Lippitsch, R., Kissling, E., & Ansorge, J. (2003). Upper mantle structure beneath the Alpine orogen from high-resolution teleseismic tomography. *Journal of Geophysical Research: Solid Earth*, *108*(B8).

Liou, J. G., Tsujimori, T., Zhang, R. Y., Katayama, I., & Maruyama, S. (2004). Global UHP metamorphism and continental subduction/collision: the Himalayan model. *International Geology Review*, *46*(1), 1-27.

Locatelli, M., Verlaguet, A., Agard, P., Pettke, T., & Federico, L. (2019). Fluid pulses during stepwise brecciation at intermediate subduction depths (Monviso eclogites, W. Alps): First internally then externally sourced. *Geochemistry, geophysics, geosystems*, *20*(11), 5285-5318.

Luisier, C., Baumgartner, L., Schmalholz, S. M., Siron, G., & Vennemann, T. (2019). Metamorphic pressure variation in a coherent Alpine nappe challenges lithostatic pressure paradigm. *Nature communications*, *10*(1), 1-11.

Luvizotto, G. L., Zack, T., Meyer, H. P., Ludwig, T., Triebold, S., Kronz, A., ... & von Eynatten, H. (2009). Rutile crystals as potential trace element and isotope mineral standards for microanalysis. *Chemical Geology*, *261*(3-4), 346-369.

Malaroda, R. (1972). Carta geologica d'Italia, 1/100.000. Argentera-Dronero.

Malusà, M. G., Polino, R., Zattin, M., Bigazzi, G., Martin, S., & Piana, F. (2005). Miocene to Present differential exhumation in the Western Alps: Insights from fission track thermochronology. *Tectonics*, *24*(3).

Manatschal, G. (2004). New models for evolution of magma-poor rifted margins based on a review of data and concepts from West Iberia and the Alps. *International Journal of Earth Sciences*, *93*(3), 432-466.

Manzotti, P., Ballèvre, M., & Poujol, M. (2016). Detrital zircon geochronology in the Dora-Maira and Zone Houillère: a record of sediment travel paths in the Carboniferous. *Terra Nova*, *28*(4), 279-288.

Manzotti, P., Bosse, V., Pitra, P., Robyr, M., Schiavi, F., & Ballèvre, M. (2018). Exhumation rates in the Gran Paradiso Massif (Western Alps) constrained by in situ U–Th–Pb dating of accessory phases (monazite, allanite and xenotime). *Contributions to Mineralogy and Petrology*, *173*(3), 1-28.

Manzotti, P., Pitra, P., Langlade, J., Ballèvre, M. (2015). Constraining P–T conditions during thrusting of a higher-pressure unit over a lower-pressure one (Gran Paradiso, Western Alps). *Journal of Metamorphic Geology*, *33*(9), 981-1002.

Markley, M. J., Teyssier, C., Cosca, M. A., Caby, R., Hunziker, J. C., & Sartori, M. (1998). Alpine deformation and [40]Ar/[39]Ar geochronology of synkinematic white mica in the Siviez-Mischabel Nappe, western Pennine Alps, Switzerland. *Tectonics*, *17*(3), 407-425.

Meffan-Main, S., Cliff, R. A., Barnicoat, A. C., Lombardo, B., & Compagnoni, R. (2004). A Tertiary age for Alpine high-pressure metamorphism in the Gran Paradiso massif, Western Alps: A Rb–Sr microsampling study. *Journal of Metamorphic Geology*, *22*(4), 267-281.

Mezger, K., Hanson, G. N., & Bohlen, S. R. (1989). High-precision UPb ages of metamorphic rutile: application to the cooling history of high-grade terranes. *Earth and Planetary Science Letters*, *96*(1-2), 106-118.

Michard, A. (1967). Etudes géologiques dans les zones internes des Alpes cottiennes. Paris, C.N.R.S., 447 p., https://tel.archives-ouvertes.fr/tel-00802836.

Michard, A., Avigad, D., Goffé, B., & Chopin, C. (2004). The high-pressure metamorphic front of the south Western Alps (Ubaye-Maira transect, France, Italy). *Schweizerische Mineralogische Petrogrographische Mitterilungen*, *84*, 215-235.

Michard, A., & Henry, C. (1988). Les Nappes briançonnaises en Haute-Ubaye (Alpes franco-italiennes); contribution à la reconstitution paléogéographique du Briançonnais au Mésozoïque. *Bulletin de la Société géologique de France*, *4*(4), 693-701.

Mohn, G., Manatschal, G., Beltrando, M., & Haupert, I. (2014). The role of rift-inherited hyper-extension in Alpine-type orogens. *Terra Nova*, *26*(5), 347-353.

Monié, P. (1990). Preservation of Hercynian [40]Ar/[39]Ar ages through high-pressure low-temperature Alpine metamorphism in the Western Alps. *European Journal of Mineralogy*, 2, 343-361.

Monié, P., & Chopin, C. (1991). ^{40}Ar/^{39}Ar dating in coesite-bearing and associated units of the Dora Maira massif, Western Alps. *European Journal of Mineralogy*, 3, 239-262.

Monié, P., & Philippot, P. (1989). Mise en évidence de l'âge éocène moyen du métamorphisme de haute-pression dans la nappe ophiolitique du Monviso (Alpes occidentales) par la méthode ^{39}Ar-^{40}Ar. *Comptes rendus de l'Académie des sciences. Série 2, Mécanique, Physique, Chimie, Sciences de l'univers, Sciences de la Terre*, *309*(2), 245-251.

Mulder, T., Callec, Y., Parize, O., Joseph P., Schneider, J. L., Robin, C., ... & Zaragosi, S. (2010). High-resolution analysis of submarine lobes deposits: Seismic-scale outcrops of the Lauzanier area (SE Alps, France). *Sedimentary Geology*, *229*(3), 160-191.

Nosenzo F., Manzotti P., Poujol M., Ballèvre M., Langlade J. (2022). A window into an older orogenic cycle: *P-T* conditions and timing of the pre-Alpine history of the Dora-Maira Massif (Western Alps). *Journal of Metamorphic Geology*.

Nowlan, E. U., Schertl, H. P., & Schreyer, W. (2000). Garnet–omphacite–phengite thermobarometry of eclogites from the coesite-bearing unit of the southern Dora-Maira Massif, Western Alps. *Lithos*, *52*(1-4), 197-214.

Pantet, A., Epard, J. L., & Masson, H. (2020). Mimicking Alpine thrusts by passive deformation of synsedimentary normal faults: a record of the Jurassic extension of the European margin (Mont Fort nappe, Pennine Alps). *Swiss Journal of Geosciences*, *113*(1), 1-25.

Paquette, J. L., Chopin, C., & Peucat, J. J. (1989). U-Pb zircon, Rb-Sr and Sm-Nd geochronology of high- to very-high-pressure meta-acidic rocks from the Western Alps. *Contributions to Mineralogy and Petrology*, *101*(3), 280-289.

Paquette, J. L., Montel, J. M., & Chopin, C. (1999). U-Th-Pb dating of the Brossasco ultrahigh-pressure metagranite, Dora-Maira massif, western Alps. *European Journal of Mineralogy*, *11*, 69-77.

Paton, C., Hellstrom, J., Paul, B., Woodhead, J., & Hergt, J. (2011). Visualization Iolite: Freeware for the visualisation and processing of mass spectrometric data. *Journal of Analytical Atomic Spectrometry*, *26*(12), 2508-2518.

Pfiffner, O. A., Ellis, S., & Beaumont, C. (2000). Collision tectonics in the Swiss Alps: Insight from geodynamic modeling. *Tectonics*, *19*(6), 1065-1094.

Platt, J. P., Behrmann, J. H., Cunningham, P. C., Dewey, J. F., Helman, M., Parish, M., ... & Weston, P. J. (1989). Kinematics of the Alpine arc and the motion history of Adria. *Nature*, *337*(6203), 158-161.

Plunder, A., Agard, P., Dubacq, B., Chopin, C., & Bellanger, M. (2012). How continuous and precise is the record of P–T paths? Insights from combined thermobarometry and thermodynamic modelling into subduction dynamics (Schistes Lustrés, W. Alps). *Journal of Metamorphic Geology*, *30*(3), 323-346.

Pognante, U., & Sandrone, R. (1989): Eclogites in the Northern Dora-Maira Nappe (Western Alps, Italy). *Mineralogy and Petrology*, *40*, 57-71.

Powell, R., Green, E. C., Marillo Sialer, E., & Woodhead, J. (2020). Robust isochron calculation. *Geochronology*, *2*(2), 325-342.

Romagny, A., Jolivet, L., Menant, A., Bessière, E., Maillard, A., Canva, A., ... & Augier, R. (2020). Detailed tectonic reconstructions of the Western Mediterranean region for the last 35 Ma, insights on driving mechanisms. *BSGF-Earth Sciences Bulletin*, 191(1), 37.

Rosenbaum, G., Menegon, L., Glodny, J., Vasconcelos, P., Ring, U., Massironi, M., ... & Nasipuri, P. (2012). Dating deformation in the Gran Paradiso Massif (NW Italian Alps): Implications for the exhumation of high-pressure rocks in a collisional belt. *Lithos*, *144*, 130-144.

Rubatto, D., & Angiboust, S. (2015). Oxygen isotope record of oceanic and high-pressure metasomatism: a P–T–time–fluid path for the Monviso eclogites (Italy). *Contributions to Mineralogy and Petrology*, *170*(5), 1-16.

Rubatto, D., & Gebauer, D. (1999). Eo/Oligocene (35 Ma) high-pressure metamorphism in the Gornergrat zone (Monte Rosa, western Alps): implications for paleogeography. *Schweizerische Mineralogische und Petrographische Mitteilungen*, *79*, 353-362.

Rubatto, D., & Hermann, J. (2001). Exhumation as fast as subduction? *Geology*, *29*(1), 3-6.

Rubatto, D., & Hermann, J. (2003). Zircon formation during fluid circulation in eclogites (Monviso, Western Alps): implications for Zr and Hf budget in subduction zones. *Geochimica et Cosmochimica Acta*, *67*(12), 2173-2187.

Sandrone, R., Cadoppi, P., Sacchi, R., & Vialon, P. (1993). The Dora-Maira Massif. In *Pre-Mesozoic geology in the Alps* (pp. 317-325). Springer, Berlin, Heidelberg.

Scaillet, S. (1996). Excess [40]Ar transport scale and mechanism in high-pressure phengites: A case study from an eclogitized metabasite of the Dora-Maira nappe, western Alps. *Geochimica et Cosmochimica Acta*, *60*(6), 1075-1090.

Scaillet, S., Féraud, G., Lagabrielle, Y., Ballèvre, M., & Ruffet, G. (1990). [40]Ar/[39]Ar laser-probe dating by step heating and spot fusion of phengites from the Dora Maira nappe of the western Alps, Italy. *Geology*, *18*(8), 741-744.

Scharf, A., Handy, M. R., Ziemann, M. A., & Schmid, S. M. (2013). Peak-temperature patterns of polyphase metamorphism resulting from accretion, subduction and collision (eastern Tauern Window, European Alps)–a study with Raman microspectroscopy on carbonaceous material (RSCM). *Journal of metamorphic Geology*, *31*(8), 863-880.

Schenker, F. L., Schmalholz, S. M., Moulas, E., Pleuger, J., Baumgartner, L. P., Podladchikov, Y., ... & Müntener, O. (2015). Current challenges for explaining (ultra) high-pressure tectonism in the Pennine domain of the Central and Western Alps. *Journal of metamorphic Geology*, *33*(8), 869-886.

Schertl, H. P., Schreyer, W., & Chopin, C. (1991). The pyrope-coesite rocks and their country rocks at Parigi, Dora Maira Massif, Western Alps: detailed petrography, mineral chemistry and PT-path. *Contributions to Mineralogy and Petrology*, *108*(1), 1-21.

Schmalholz, S. M., Duretz, T., Schenker, F. L., & Podladchikov, Y. Y. (2014). Kinematics and dynamics of tectonic nappes: 2-D numerical modelling and implications for high and ultra-high pressure tectonism in the Western Alps. *Tectonophysics*, *631*, 160-175.

Schmalholz, S. M., & Schenker, F. L. (2016). Exhumation of the Dora Maira ultrahigh-pressure unit by buoyant uprise within a low-viscosity mantle oblique-slip shear zone. *Terra Nova*, *28*(5), 348-355.

Schmid, S. M., Pfiffner, O. A., Froitzheim, N., Schönborn, G., & Kissling, E. (1996). Geophysical-geological transect and tectonic evolution of the Swiss-Italian Alps. *Tectonics*, *15*(5), 1036-1064.

Schmitz, M. D., & Bowring, S. A. (2001). U-Pb zircon and titanite systematics of the Fish Canyon Tuff: an assessment of high-precision U-Pb geochronology and its application to young volcanic rocks. *Geochimica et Cosmochimica Acta*, *65*(15), 2571-2587.

Schmitz, M. D., & Schoene, B. (2007). Derivation of isotope ratios, errors, and error correlations for U-Pb geochronology using ^{205}Pb-^{235}U-(^{233}U)-spiked isotope dilution thermal ionization mass spectrometric data. *Geochemistry, Geophysics, Geosystems*, *8*(8).

Schwartz, S., Lardeaux, J. M., Guillot, S., & Tricart, P. (2000a). Diversité du métamorphisme éclogitique dans le massif ophiolitique du Monviso (Alpes occidentales, Italie). *Geodinamica Acta*, *13*(2-3), 169-188.

Schwartz, S., Lardeaux, J. M., & Tricart, P. (2000b). La zone d'Acceglio (Alpes cottiennes) : un nouvel exemple de croûte continentale éclogitisée dans les Alpes occidentales. *Comptes Rendus de l'Académie des Sciences-Series IIA-Earth and Planetary Science*, *330*(12), 859-866.

Sharp, Z.D., Essene, E.J., & Hunziker J.C. (1993). Stable isotope geochemistry and phase equilibria of coesite-bearing whiteschists, Dora Maira Massif, western Alps. *Contributions to Mineralogy and Petrology*, *114*, 1-12.

Simon-Labric, T., Rolland, Y., Dumont, T., Heymes, T., Authemayou, C., Corsini, M., & Fornari, M. (2009). ^{40}Ar/^{39}Ar dating of Penninic Front tectonic displacement (W Alps) during the Lower Oligocene (31–34 Ma). *Terra Nova*, *21*(2), 127-136.

Söderlund, U., Patchett, P. J., Vervoort, J. D., & Isachsen, C. E. (2004). The ^{176}Lu decay constant determined by Lu–Hf and U–Pb isotope systematics of Precambrian mafic intrusions. *Earth and Planetary Science Letters*, *219*(3-4), 311-324.

Soret, M., Larson, K. P., Cottle, J., & Ali, A. (2021). How Himalayan collision stems from subduction. *Geology, 49*(8), 894-898.

Spandler, C., Hammerli, J., Sha, P., Hilbert-Wolf, H., Hu, Y., Roberts, E., & Schmitz, M. (2016). MKED1: a new titanite standard for in situ analysis of Sm–Nd isotopes and U–Pb geochronology. *Chemical Geology*, *425*, 110-126.

Spencer, K. J., Hacker, B. R., Kylander-Clark, A. R. C., Andersen, T. B., Cottle, J. M., Stearns, M. A., ... & Seward, G. G. E. (2013). Campaign-style titanite U–Pb dating by laser-ablation ICP: Implications for crustal flow, phase transformations and titanite closure. *Chemical Geology*, *341*, 84-101.

Stacey, J. S., & Kramers, J.D. (1975). Approximation of terrestrial lead isotope evolution by a two-stage model. *Earth and Planetary Science Letters*, *26*(2), 207-221.

Strzerzynski, P., Guillot, S., Leloup, P. H., Arnaud, N., Vidal, O., Ledru, P., ... & Darmendrail, X. (2012). Tectono-metamorphic evolution of the Briançonnais zone (Modane-Aussois and southern Vanoise units, Lyon Turin transect, western Alps). *Journal of Geodynamics*, *56*, 55-75.

Syracuse, E. M., van Keken, P. E., & Abers, G. A. (2010). The global range of subduction zone thermal models. *Physics of the Earth and Planetary Interiors*, *183*(1-2), 73-90

Tian, Y., Xiao, Y., Chen, Y. X., Sun, H., Liu, H., Tong, F., ... & Schertl, H. P. (2019). Serpentinite-derived low δ^7Li fluids in continental subduction zones: Constraints from the fluid metasomatic rocks (whiteschist) from the Dora-Maira Massif, Western Alps. *Lithos*, *348*, 105177.

Tilton, G. R., Schreyer, W., & Schertl, H. P. (1989). Pb-Sr-Nd isotopic behavior of deeply subducted crustal rocks from the Dora Maira Massif, Western Alps, Italy. *Geochimica et Cosmochimica Acta*, *53*(6), 1391-1400.

Tilton, G. R., Schreyer, W., & Schertl, H. P. (1991). Pb–Sr–Nd isotopic behavior of deeply subducted crustal rocks from the Dora Maira Massif, Western Alps, Italy-II: what is the age of the ultrahigh-pressure metamorphism? *Contributions to Mineralogy and Petrology*, *108*(1), 22-33.

Tomkins, H. S., Powell, R., & Ellis, D. J. (2007). The pressure dependence of the zirconium-in-rutile thermometer. *Journal of metamorphic Geology*, *25*(6), 703-713.

Tricart, P., Van der Beek, P., Schwartz, S., & Labrin, E. (2007). Diachronous late-stage exhumation across the western Alpine arc: constraints from apatite fission-track thermochronology between the Pelvoux and Dora-Maira Massifs. *Journal of the Geological Society*, *164*(1), 163-174.

Vermeesch, P. (2018). IsoplotR: A free and open toolbox for geochronology. *Geoscience Frontiers*, *9*(5), 1479-1493.

Vialette, Y., & Vialon, P. (1964). Etude géochronologique de quelques micas des formations du massif Dora-Maira, Alpes cottiennes piémontaises. *Ann Fac Sc Clermont-Ferrand Et Géochron I*, 91-99.

Vialon, P. (1966). *Etude géologique du massif cristallin Dora-Maira : Alpes cottiennes internes : Italie* (Doctoral dissertation, Université de Grenoble).

Vignaroli, G., Faccenna, C., Jolivet, L., Piromallo, C., & Rossetti, F. (2008). Subduction polarity reversal at the junction between the Western Alps and the Northern Apennines, Italy. *Tectonophysics*, *450*(1-4), 34-50.

Villa, I. M., Bucher, S., Bousquet, R., Kleinhanns, I. C., & Schmid, S. M. (2014). Dating polygenetic metamorphic assemblages along a transect across the Western Alps. *Journal of Petrology*, *55*(4), 803-830.

Vry, J. K., & Baker, J. A. (2006). LA-MC-ICPMS Pb–Pb dating of rutile from slowly cooled granulites: confirmation of the high closure temperature for Pb diffusion in rutile. *Geochimica et Cosmochimica Acta*, *70*(7), 1807-1820.

Wain, A. (1997). New evidence for coesite in eclogite and gneisses: Defining an ultrahigh-pressure province in the Western Gneiss region of Norway. *Geology*, *25*(10), 927-930.

Wiederkehr, M., Bousquet, R., Schmid, S. M., & Berger, A. (2008). From subduction to collision: thermal overprint of HP/LT meta-sediments in the north-eastern Lepontine Dome (Swiss Alps) and consequences regarding the tectono-metamorphic evolution of the Alpine orogenic wedge. *Swiss Journal of Geosciences*, *101*(1), 127-155.

Xiong J.W., Chen, Y. X., Zhou, K., Schertl, H. P., Zheng, Y. F., Huang, F., ... & Chen, Z. W. (2021). Fe and O isotopes in coesite-bearing jadeite quartzite from the Western Alps record multistage fluid-rock interactions in a continental subduction zone. *Geochimica et Cosmochimica Acta*, *312*, 1-24.

York, D. (1967). The best isochron. *Earth and Planetary Science Letters*, *2*(5), 479-482.

Zack, T., Moraes, R., & Kronz, A. (2004). Temperature dependence of Zr in rutile: empirical calibration of a rutile thermometer. *Contributions to Mineralogy and Petrology*, *148*(4), 471-488.

Zack, T., Kronz, A., Foley, S. F., & Rivers, T. (2002). Trace element abundances in rutiles from eclogites and associated garnet mica schists. *Chemical Geology*, *184*(1-2), 97-122.

Zechmeister, M. S., Ferré, E. C., Cosca, M. A., & Geissman, J. W. (2007). Slow and fast deformation in the Dora Maira Massif, Italian Alps: Pseudotachylytes and inferences on exhumation history. *Journal of Structural Geology*, *29*(7), 1114-1130.

Zhao, L., Malusà, M. G., Yuan, H., Paul, A., Guillot, S., Lu, Y., ... & Bodin, T. (2020). Evidence for a serpentinized plate interface favouring continental subduction. *Nature communications*, *11*(1), 1-8.

Zhao, L., Paul, A., Guillot, S., Solarino, S., Malusà, M. G., Zheng, T., ... & Wang, Q. (2015). First seismic evidence for continental subduction beneath the Western Alps. *Geology*, *43*(9), 815-818.

Ziegler, P. A. (1992). European Cenozoic rift system. *Tectonophysics*, *208*(1-3), 91-111.